END
DATE
FILMED
5-80
DTIC

MICROCOPY RESOLUTION TEST CHART
NATIONAL BUREAU OF STANDARDS-1963-A

AD

ADA083387

CHEMICAL SYSTEMS LABORATORY CONTRACTOR REPORT
ARCSL-CR-80009

DEVELOPMENT STUDY OF A
TWO-STAGE CONTINUOUS FLOW IMPACTOR

Final Report

by

Nahum Gat

March, 1980

TRW DEFENSE AND SPACE SYSTEMS GROUP
One Space Park
Redondo Beach, CA 90278

Contract Number DAAK11-78-C-0103

US ARMY ARMAMENT RESEARCH AND DEVELOPMENT COMMAND
Chemical Systems Laboratory
Aberdeen Proving Ground, Maryland 21010

Approved for public release; distribution unlimited.

DC FILE COPY

80 3 27 015

Disclaimer

The views, opinions and/or findings contained in this report
are those of the authors and should not be construed as an official
Department of the Army position, policy or decision unless so desig-
nated by other documentation.

Disposition

Destroy this report when it is no longer needed. Do not return
it to the originator.

CHEMICAL SYSTEMS LABORATORY CONTRACTOR REPORT
ARCSL-CR-80009

DEVELOPMENT STUDY OF A
TWO-STAGE CONTINUOUS FLOW IMPACTOR

Final Report

by

Nahum Gat

March, 1980

TRW DEFENSE AND SPACE SYSTEMS GROUP
One Space Park
Redondo Beach, CA 90278

Contract Number DAAK11-78-C-0103

US ARMY ARMAMENT RESEARCH AND DEVELOPMENT COMMAND
Chemical Systems Laboratory
Aberdeen Proving Ground, Maryland 21010

Approved for public release; distribution unlimited.

DTIC
ELECTE
APR 24 1980

B

REPORT DOCUMENTATION PAGE		READ INSTRUCTIONS BEFORE COMPLETING FORM
1. REPORT NUMBER ARCSL-CR-80009	2. GOVT ACCESSION NO.	3. RECIPIENT'S CATALOG NUMBER
4. TITLE (and Subtitle) DEVELOPMENT STUDY OF A TWO-STAGE CONTINUOUS FLOW IMPACTOR		5. TYPE OF REPORT & PERIOD COVERED Final Report
		6. PERFORMING ORG. REPORT NUMBER 33437-6001-RU-00
7. AUTHOR(s) Nahum Gat		8. CONTRACT OR GRANT NUMBER(s) DAAK11-78-C-0103 *new*
9. PERFORMING ORGANIZATION NAME AND ADDRESS TRW Defense and Space Systems Group One Space Park, Redondo Beach, CA 90278		10. PROGRAM ELEMENT, PROJECT, TASK AREA & WORK UNIT NUMBERS
11. CONTROLLING OFFICE NAME AND ADDRESS Commander/Director, Chemical Systems Laboratory ATTN: DRDAR-CLJ-R Aberdeen Proving Ground, Maryland 21010		12. REPORT DATE March 1980
		13. NUMBER OF PAGES
14. MONITORING AGENCY NAME & ADDRESS(if different from Controlling Office) Commander/Director, Chemical Systems Laboratory ATTN: DRDAR-CLB-PS Aberdeen Proving Ground, Maryland 21010		15. SECURITY CLASS. (of this report) UNCLASSIFIED
		15a. DECLASSIFICATION/DOWNGRADING SCHEDULE

16. DISTRIBUTION STATEMENT (of this Report)

Approved for public release; distribution unlimited.

17. DISTRIBUTION STATEMENT (of the abstract entered in Block 20, if different from Report)

18. SUPPLEMENTARY NOTES

Contract Project Officer: Robert Doherty (DRDAR-CLB-PS, 67--2760)

19. KEY WORDS (Continue on reverse side if necessary and identify by block number)

Particles	Cascade
Aerosol	Impactor
Separation	
Impactor	

micron

20. ABSTRACT (Continue on reverse side if necessary and identify by block number)

Two units of a Continuous Flow Impactor (CI) were designed, constructed and tested. The units have been calibrated using DOP droplets and their fractionation points are approximately 4 and 1 μm for the first and second unit respectively. The principal design criteria established in previous studies have been verified, and reshaping the collection chambers has proven effective in improving performance. The steepness of the cross-over efficiency of the 1st unit is comparable to that of other commercially available impactors. The performance of the 2nd unit is not as good though; this is attributed to (cont)

DD FORM 1473 1 JAN 73   EDITION OF 1 NOV 65 IS OBSOLETE

20. Abstract (continued)

high particle loss in that unit.

The two units have been operated in a cascade arrangement which separates an airborne "window" of a desired particle size range - between the fractionation points of the two stages - out of a polydispersed aerosol.

The particle loss mechanisms are discussed and improvements are suggested to reduce the loss. Other potential applications of the CI such as in the separation of monodispersed aerosols, density measurement of spherical particles and shape factor determination are discussed as well.

PREFACE

The work reported herein was accomplished from March 1979 to September 1979. It was authorized under contract DAAK11-78-C-0103 entitled Development Study of a Two-Stage Continuous Flow Impactor.

Reproduction of this report in whole or in part is prohibited except with permission of the Commander/Director, Chemical Systems Laboratory, Attn: DRDAR-CLJ-R, Aberdeen Proving Ground, MD 21010. However, Defense Documentation Center and the National Technical Information Service are authorized to reproduce the document for U.S. Government purposes.

The use of trade names in this report does not constitute an official endorsement or approval of the use of such commerical hardware or software. This report may not be cited for purposes of advertisement.

ACCESSION for		
NTIS	White Section	✓
DDC	Buff Section	☐
UNANNOUNCED		☐
JUSTIFICATION		
BY		
DISTRIBUTION/AVAILABILITY CODES		
Dist.	AVAIL. and/or SPECIAL	
A		

3

TABLE OF CONTENTS

LIST OF FIGURES

DEVELOPMENT STUDY OF A TWO-STAGE CONTINUOUS FLOW IMPACTOR

1. INTRODUCTION

The increasing interest in recent years in the field of aerosols
created the need for and spurred the development of better techniques
for particulate sampling, sizing and analysis. Often, the size
distribution of an aerosol is of a primary interest. Conventional
impactors are used for the classification of airborne particulates into
size groups and for the collection of these particulates on impaction
surfaces. The size fractionation in the impactor is done by the acceleration of
the particulates and the carrier gas towards a stagnation surface. The
large particulates (or more accurately, those with a high momentum) impact
upon the surface which is coated with grease to capture them. Small
particulates follow the gas stream lines around the obstacle and are carried
away by the gas. Further fractionation can be done by an increase in the velocity
of the particulates in subsequent impactor stages. The actual count
of the particulate matter, shape analysis and physical/chemical assay
is done utilizing electro/optical techniques, spectrometry, etc. This
subject is discussed in several review articles such as by Lapple (1968),
Austin (1979), Lee et al (1979), and Dzubay and Stevens (1975).

Utilizing the same principle of operation as in the conventional
impactor, the particulates in a virtual impactor accelerate towards a
gaseous interface separating the aerosol stream from a "clean" chamber
(see for instance, Hounam and Sherwood 1965, Conners 1966, Loo and
Jaklevic 1973, Loo et al 1976, and McFarland et al 1978). A small
fraction of the incoming aerosol carrying gas is allowed to enter the
"clean" chamber, while the rest of the gas is forced to turn and flow
around the inlet to the "clean" chamber. Here, again, heavy particulates

cì ̦ s the interface while small ones are carried away by the deflected flow. The particulates from both streams are collected eventually on filter membranes for further analysis. This device is often called a dichotomous sampler.

Not having a solid collection surface directly exposed to the incoming stream, the virtual impactor avoids the problem of particulate bouncing and re-entrainment. Also avoided is the need for a sticky surface, coated with various chemicals to capture the particulates. Such chemicals may induce chemical and physical changes in the captured materials.

In the opposing jets classifier, a gaseous interface separates two collection chambers as in the virtual impactor. Some differences exist, however,as discussed below. The concept of particulates separation using opposing jets was suggested by Luna (1965) and further pursued by others (Hall, 1970 and Mears, 1973). Brooks et al (1979) developed an opposing jets classifier, termed a Continuous Flow Impactor (CI), which allows a detailed parametric study of its performance. The CI has proven the feasibility of utilizing the concept in practice. A similar device was built and tested by Willeke and Pavlik (1978).

The principle of operation of the CI is illustrated schematically in Figure 1. A particle laden gas (aerosol) jet and an identical clean gas jet collide in the plane of the splitter plate, forming a gaseous interface between the two collection chambers. For well balanced jets, and as long as the interface is stable, there is no gaseous cross-over from one side to the other. Inertial fractionation is achieved thus,
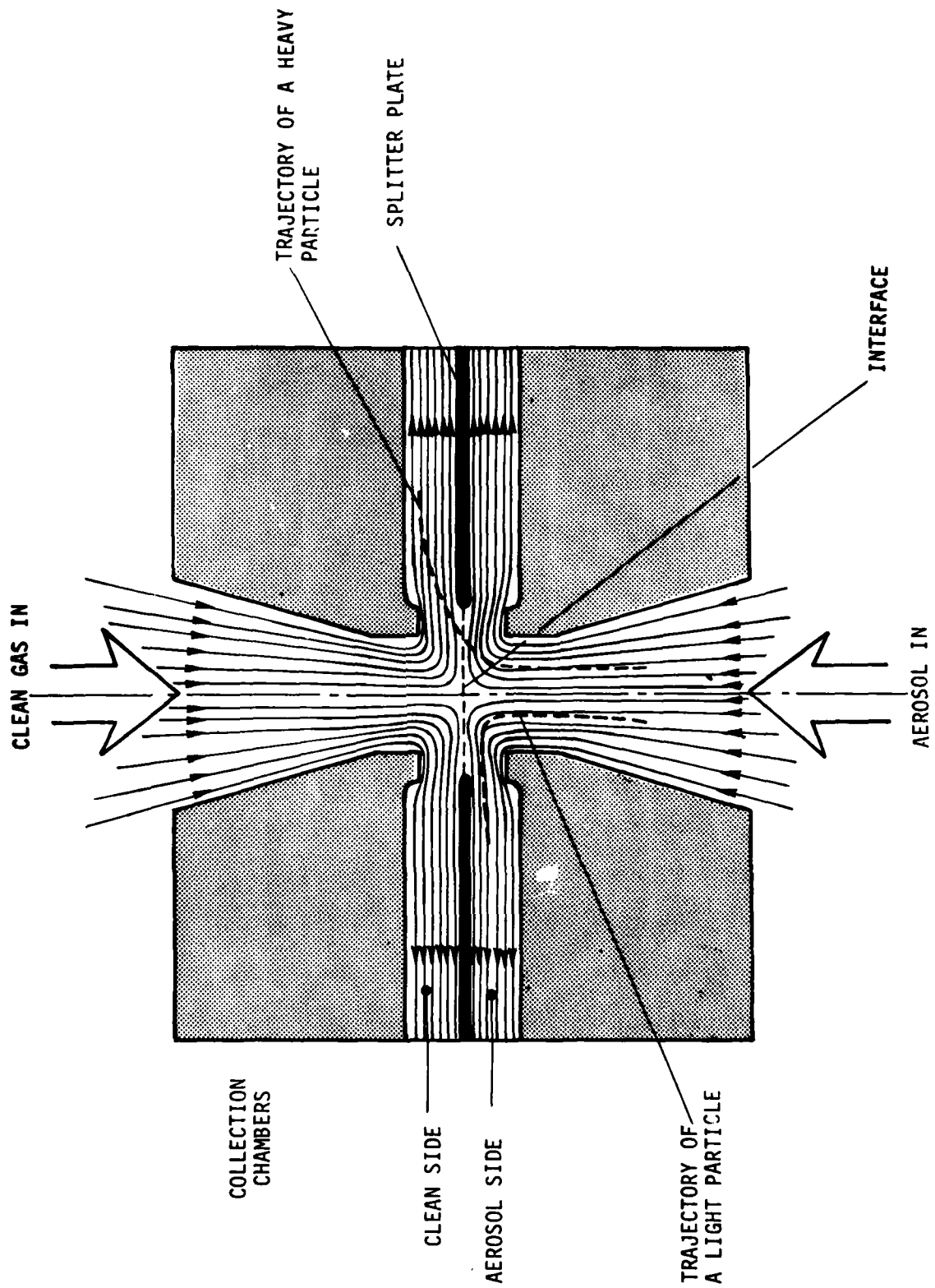
Figure 1: Continuous Impactor - Principle of Operation

TRAJECTORY OF A HEAVY PARTICLE

SPLITTER PLATE

INTERFACE

CLEAN GAS IN

AEROSOL IN

COLLECTION CHAMBERS

CLEAN SIDE

AEROSOL SIDE

TRAJECTORY OF A LIGHT PARTICLE

by controlling the velocity of the incoming streams. The heavy particles in the aerosol stream cross over the interface into the "clean" collection chamber while light particles follow the stream lines and remain in the aerosol side chamber, as shown by the dashed lines in Figure 1. Some of the advantages and the shortcomings of the CI are briefly mentioned next.

The efficiency of the CI is a function of the particle size and it is a measure of the fraction of particles of a given size which cross over and leave the CI through the clean chamber side. A CI is designed to operate around a so called 50 per cent fractionation size. Typically, the efficiency of the CI (or of any other impactor) is high for particles larger than the 50% fractionation size and it is low for particles smaller than that size. In theory all the large particles in the aerosol stream cross over to the clean side. In practice, however, there is a possibility that a heavy particle traveling along the axis of the jet may penetrate far upstream into the clean jet, then come to a brief stop and eventually trajected back into the aerosol side. Hence, the expected efficiency for large particles is less than 100%. The actual value depends among other things upon the radial distribution of the particles in the inlet nozzle.

For small particles, the expected efficiency is 0% since for a well balanced flow there is no gas cross-over and the small particles remain in the original stream. For the dichotomous impactor, Conners (1966) found that there is an optimal fraction of the flow which has to be allowed into the clean chamber. A too low or a too high fraction of the flow produces poor separation efficiency. Also, the fraction of flow entering the clean side chamber always carries with it some small

particles. This sets a lower limit to the small particle cross over
efficiency, this limit is around 5-15% in McFarland's report (1978).
It is unclear, however, how sensitive the performance of the CI is to
a small inbalance in the two jets. Also the performance of the CI
may suffer from interface instabilities which allow gas cross over and
which disrupt the proper operation of the CI. This problem can be
taken care of, though, by a proper design of the apparatus (Luna, 1965;
Brooks et al, 1979). Another apparent advantage of the CI is in the
possibility to shift the fractionation efficiency curve merely by
controlling the flow rate of the two jets.

When it is desirable to classify particulates while maintaining them
in suspension in a gas (e.g., for introduction into an optical particle
counter or for the separation of a monodispersed aerosol out of a polydispersed
aerosol), the CI has an additional advantage. The separated particulates
leave the CI entrained in a gas stream of the same flow rate as at the
inlet to the device.

With the latter advantage in mind, the purpose of the present
investigation was to study the possibility of a cascade, 2-stage CI operation,
arranged in such a way that a "window" of a desired particle size range
(still as an aerosol) can be obtained. That can be achieved by directing the
flow leaving the first stage into a second stage which has a different fractionation
point. Explicitly, stage one separates an incoming stream of a polydispersed
aerosol into two streams of aerosol. One, with particle size above the
fractionation point and the other with particles below that point. The
latter stream enters into a second stage and is again separated into two
streams. The fractionation point in the second stage being smaller than

13

that in the first stage. Thus, one stream leaving the second stage contains the smallest particles while the other stream contains particles in a "window" between the fractionation points of the two stages.

2. DESIGN

The CI design is based upon the optimization of the first prototype CI, performed by Brooks et.al. (1979). One of the design objectives in the present study was to have a simple and a cheap instrument without compromizing its performance. Figures 2 and 3 show an assembled stage of the CI and its components, respectively. The dimension of the CI can be found in Figure 4.

In the following section details are given pertinent to the semiempirical design of the impactor. This is followed by calculations of the particle dynamics in the nozzle. The analysis is used to support the semiempirical design criteria.

2.1 Parametric Impactor Design

The parameters identified as important to the operation of the CI, based upon the diameter of the jet nozzle (D), are listed by their numerical values below (see Brooks et.al., 1979).

- Spacing between the jet exit and the splitter plate-- $\ell/D = 0.75$
- Length of the straight section of the nozzle-- $N/D = 1.00$
- The diameter of the hole in the splitter plate-- $W/D = 1.25$

The latter figure was adopted from Pavlik (1978).

The determination of the nozzle diameter, D, is based upon the particle Stokes number and the gas flow rate. The Stokes number is defined as,

$$Stk = \frac{\rho_p \, d_p^2 \, U \, C}{18\mu \, (D/2)} ,$$ (1)

14
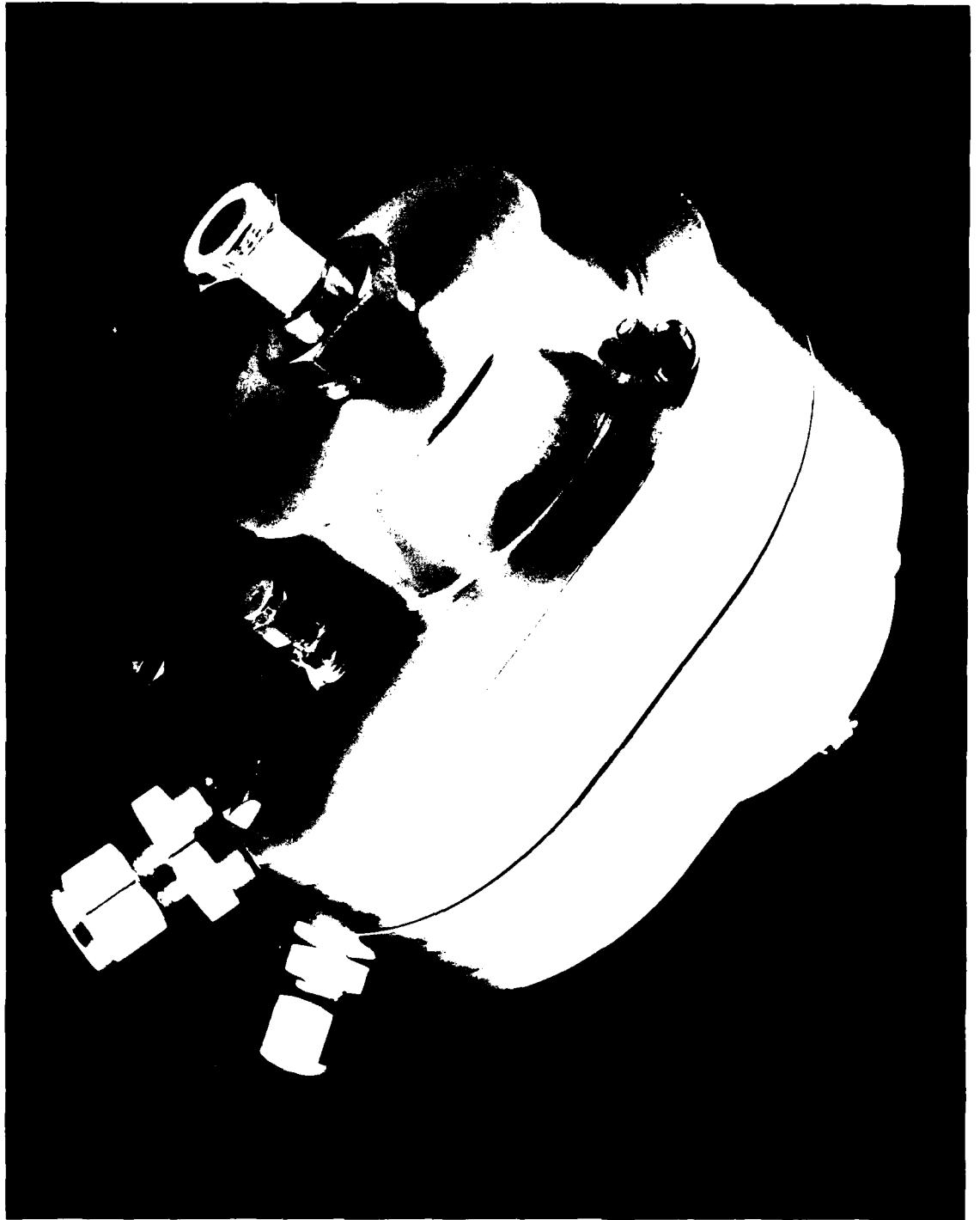
Figure 2. Continuous Impactor Assembly

Figure 3. Continuous Imapctor - Exploded View

and the jet velocity is

$$U = Q/\frac{\pi D^2}{4} \ . \tag{2}$$

Using equation (2), the Stokes number becomes

$$Stk = \frac{4}{9} \cdot \frac{\rho_p \ Q \ d_p^2 \ C}{\pi \mu \ D^3} \ , \tag{3}$$

And equation (4) gives the required nozzle diameter for a desired fractionation point, $d_{p,50\%}$;

$$D = \left[\frac{4}{9} \cdot \frac{\rho_p \ Q \ C}{\pi \mu \ Stk_{50\%}} \ d_{p,50\%}^2\right]^{1/3} \tag{4}$$

In the present design, nominal fractionation points of 4.0 and 1.5 μm were selected for the first and second stage, respectively. The value of the Stokes number for a CI of the above specified geometry, was obtained experimentally (Brooks et al., (1979)) and found to be $\sqrt{Stk_{50\%}} = 0.63$. For a flow rate of 28.3 liters/min (1 CFM), the nozzle diameters are 0.541 and 0.256 cm for the first and second stages, respectively. These numbers are slightly adjusted (by $\pm$ 1%) to allow the use of standard tools for the fabrication. The corresponding jet velocities are 2051 and 9021 cm/sec and the jet Reynolds numbers are 7553 and 15930, where

$$Re = \frac{\rho U D}{\mu}.$$

In the first CI prototype, the gas was withdrawn from the collection chambers through exit tubes inserted radially into the chambers, close to the splitter plate. It is believed that this technique of gas withdrawal could cause unnecessary particle loss. Also, since the tip of these exit tubes is

17

No.	#	H	D_{Dia}	N	ℓ
1	2	0.0	.213	.214+	.160
2	2	.084	.101	.101+	.076
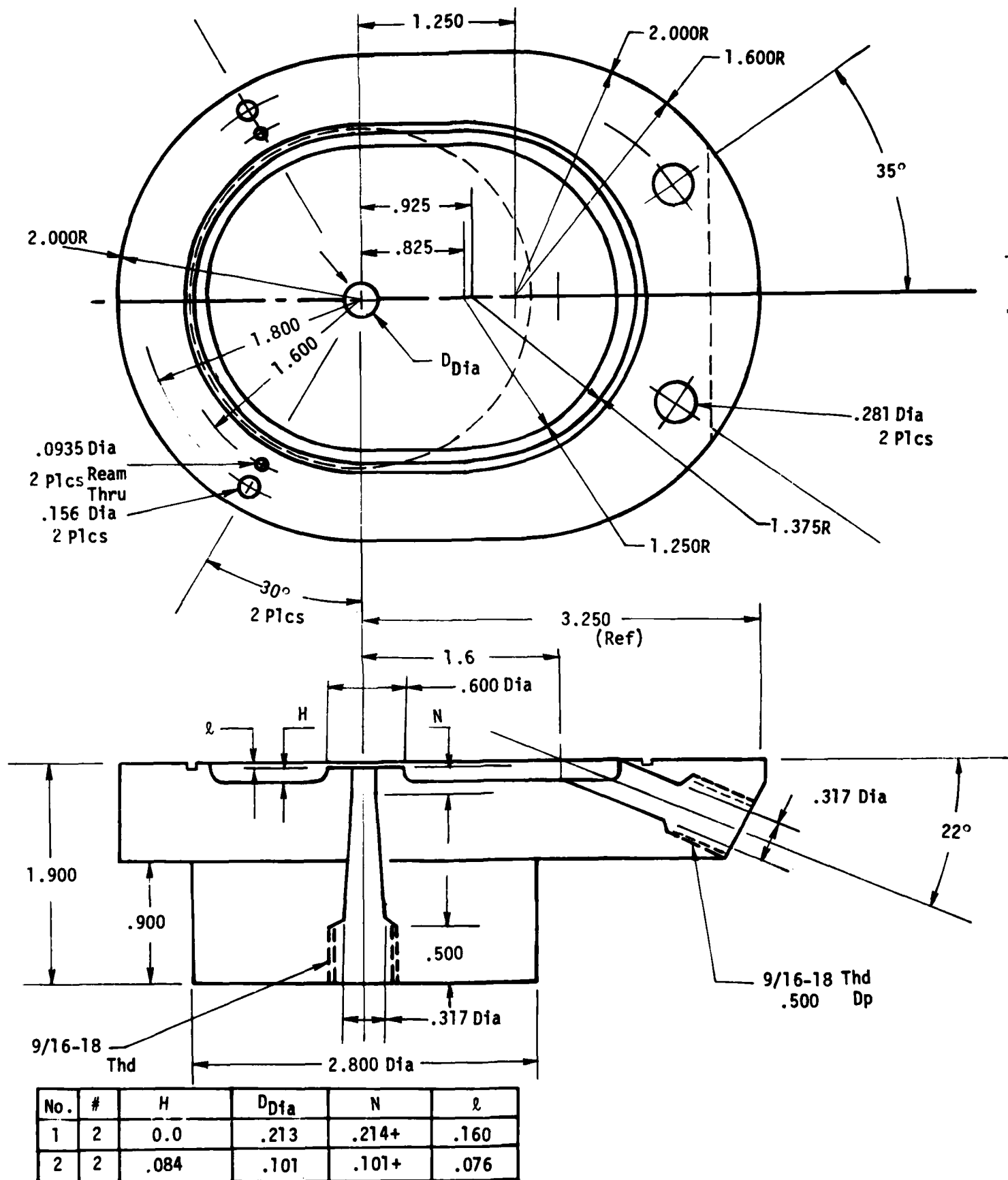
Figure 4. Continuous Impactor Design (All Dimensions are in Inches)

positioned at a radial location approximately midway between the jet exit and the collection chamber wall, the axial symmetry of the jets could be distorted, further affecting the performance curves.

In the present design, the collection chamber is given an oblong shape with the exit ports as far as possible from the jets, to minimize distortion due to the inherent non-symmetry.

2.2 Particle Dynamics in the Nozzle

The gas enters the CI through a tapered inlet section which turns into a straight nozzle close to the exit (see Figure 4). The favorable pressure gradient in the nozzle eliminates problems of flow separation and similar difficulties. In the tapered section the gas accelerates and the entrained particulates may or may not lag behind the gas, depending upon their initial conditions, size etc. In the straight section of the nozzle the gas flows at a constant velocity and the particles should have sufficient time to accommodate to the gas velocity. The flow Reynolds number in the nozzle is between 5,000 to 20,000. Since the entrance to the nozzle is almost disturbance free, the onset of turbulence, according to Schlichting (1968), may occur at a critical Reynolds number of 10,000 or over (in the case of a sharp entrance, $Re_c \simeq 2300$). Hence the nozzle may operate in a transition regime between laminar and turbulent flow.

Particle dynamics in the nozzle can be determined for the tapered and for the straight sections separately. The equation of motion for a particle in a 1-D flow is

$$m_p \frac{dV_p}{dt} = C_D \frac{1}{2} \rho (V_g - V_p)^2 A_p. \qquad (5)$$

19

Assuming flow in the Stokes regime (Reynolds number based upon the relative velocity between the gas and particle < 2), the drag coefficient is,

$$C_D = \frac{24}{Re} = \frac{24\,\mu}{\rho(V_g - V_p)d_p} \qquad (6)$$

If Re > 2, other equations apply and the drag coefficient is larger than that predicted by equation (6), (see for instance Schlichting, 1968, P. 17 or Torobin and Gauvin, 1959, P. 136). The calculation based upon the Stokes equation is, therefore, conservative .

Using the following relationships,

$$A_p = \frac{\pi d_p^2}{4} \qquad (7)$$

and

$$m_p = \rho_p \frac{\pi d_p^3}{6} \qquad (8)$$

equation (5) can be rearranged to yield

$$\frac{dV_p}{dt} = \frac{18\mu}{\rho_p\, d_p^2}\, (V_g - V_p). \qquad (9)$$

Or

$$\boxed{\frac{dV_p}{dt} = \frac{V_g - V_p}{\tau}} \qquad (10)$$

where

$$\tau = \frac{\rho_p\, d_p^2}{18\mu} \qquad (11)$$

is the particle characteristic time. In the above equations and in subsequent ones, the Cunningham slip correction to particle drag is neglected since it becomes significant only for particles smaller than one micron.

In equation (10), V_g is constant for the straight section of the inlet nozzle and it varies with the location in the tapered section. Solution to equation (10) yields the gas/particle relative motion relationship, this information is pertinent to the required length of the nozzle. It should be mentioned, however, that other considerations (e.g., the velocity profile in the nozzle) may affect the design as well.

2.2.1 Tapered Section

In the tapered section, the variation of the gas velocity is inversely proportional to the cross section area (for an incompressible gas).

$$V_g(X) = \frac{4Q}{\pi D(X)^2} \tag{12}$$

where

$$D(X) = D_1 - \frac{D_1 - D_2}{S} X . \tag{13}$$

Therefore

$$V_g(X) = \frac{4Q}{\pi D_1^2} \cdot \frac{1}{\left[1 - (1 - \frac{D_2}{D_1}) \frac{X}{S}\right]^2} \tag{14}$$

$$= \frac{V_{g_1}}{\left[1 - (1 - \frac{D_2}{D_1}) \frac{X}{S}\right]^2}$$

Where Figure 5 explains the nomenclature.

21
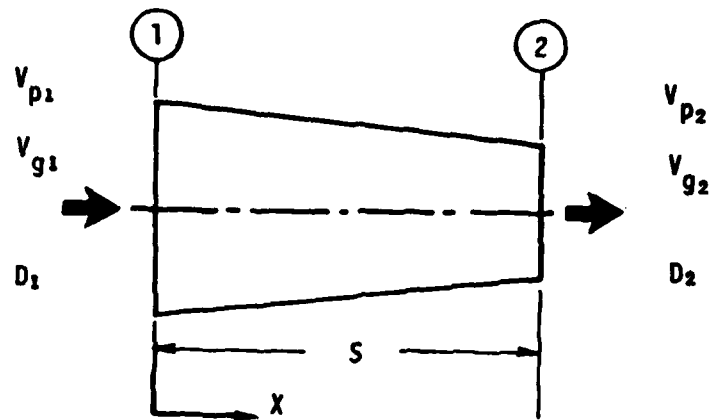
FIGURE 5 Schematic of Tapered Inlet Section .
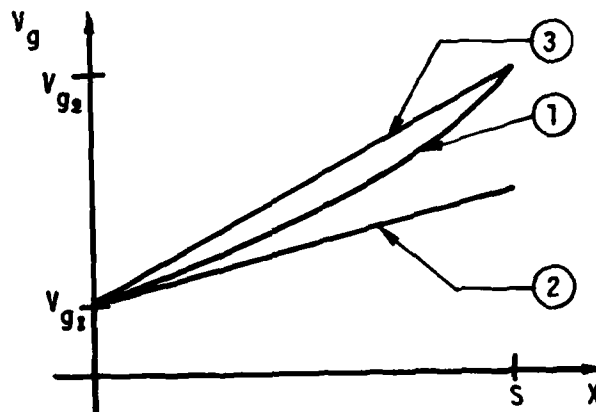
1 Actual Velocity in Nozzle

2 Taylor Expansion, 1st Order

3 Linear Approximation

FIGURE 6. Expansion of the V_g Formula.

Substitution of Equation (14) in Equation (10) gives,

$$\frac{dV_p}{dt} + \frac{V_p}{\tau} = \frac{V_{g_1}/\tau}{\left[1 - (1 - \frac{D_2}{D_1})\frac{X}{S}\right]^2} \tag{15}$$

Equation (15) is a non-linear differential equation which can be solved by making a few approximations.

Since $\left|(1 - \frac{D_2}{D_1})\frac{X}{S}\right| < 1$, the right hand side of Equation 15 can be expanded as follows

$$\left[1 - (1 - \frac{D_2}{D_1})\frac{X}{S}\right]^{-2} \approx 1 + 2(1 - \frac{D_2}{D_1})\frac{X}{S} - \ldots \tag{16}$$

Higher order terms are ignored since they again introduce nonlinearity into the equation. The error involved is of the order of $(1 - \frac{D_2}{D_1})^2 \sim 11\%$ in the first stage of the CI.

A better approximation, yet, is obtained by assuming a linear velocity variation along the nozzle as follows:

$$V_g(X) = V_{g_1}\left[1 + \left(\frac{V_{g_2}}{V_{g_1}} - 1\right)\frac{X}{S}\right] \tag{17}$$

Figure 6 shows schematically the relationship between the various approximations and actual velocity along the nozzle.

Substituting Equation (17) in Equation (10), yields

$$\frac{dV_p}{dt} + \frac{V_p}{\tau} = \frac{V_{g_1}}{\tau}\left[1 + \left(\frac{V_{g_2}}{V_{g_1}} - 1\right)\frac{X}{S}\right]. \tag{18}$$

23

Replacing the velocity terms in Equation (18) with a derivative of the distance and using a dot convention to designate time derivatives (e.g. $\dot{x} \equiv \frac{dx}{dt}$), Equation (18) is rewritten as

$$\ddot{X}_p + \frac{1}{\tau}\dot{X}_p - \frac{V_{g_1}}{\tau}\,\alpha\,\frac{X}{S} = \frac{V_{g_1}}{\tau} \tag{19}$$

Where

$$\alpha = \frac{V_{g_2}}{V_{g_1}} - 1. \tag{20}$$

Next, Equation 19 is multiplied by $\dfrac{S}{V_{g_1}^2}$ and after re-arrangement it becomes,

$$\boxed{\ddot{X}_p^* + \frac{1}{\tau^*}\dot{X}_p^* - \frac{\alpha}{\tau^*}X_p^* = \frac{1}{\tau^*}} \tag{21}$$

Where

$$X^* = X/S, \quad \tau^* = \tau/t_1, \quad t^* = t/t_1, \quad t_1 = S/V_{g_1},$$

and

$$\alpha = V_{g_2}^* - 1. \tag{20a}$$

The Boundary Conditions (BC) are,

$$\left.\begin{array}{l} X_p^*(0) = 0 \\[2mm] \dot{X}_p^*(0) = V_{p_1}^* \end{array}\right\} \quad \cdot \quad \cdot \quad \cdot \quad \cdot \quad \cdot \tag{22}$$

and

Where $V_{p_1}^* = V_{p_1}/V_{g_1}$.

The solution to Equation (21) is

$$X_p^* = C_1 \cdot \exp(\gamma_1 t^*) + C_2 \cdot \exp(\gamma_2 t^*) - \frac{1}{\alpha} \qquad (23)$$

where C_1 and C_2 are constants of integration and γ_1 and γ_2 are the solution to the characteristic equation,

$$\gamma^2 + \frac{1}{t^*} \gamma - \frac{\alpha}{\tau^*} = 0, \qquad (24)$$

i.e.,

$$\gamma_{1,2} = \frac{-1 \pm \sqrt{1+4\alpha\tau^*}}{2\tau^*} \qquad . \qquad (25)$$

For small particles, τ^* is very small, hence, approximately

$$(1+4\alpha\tau^*)^{\frac{1}{2}} \approx 1+2\alpha\tau^* - 4\alpha^2\tau^{*2} + \ldots$$

Thus

$$\gamma_1 = -\frac{1}{\tau^*} - \alpha + O(\tau^{*2})$$

and

$$\gamma_2 = \alpha + O(\tau^{*2}),$$

where the order of the error is indicated in parenthesis.

Substitution of the BC in the solution, gives

$$C_1 + C_2 = \frac{1}{\alpha}$$

and

$$\gamma_1 C_1 + \gamma_2 C_2 = V_{p_1}^*.$$

Using the approximate solutions for γ_1 and γ_2, the constants of integration are obtained,

$$C_1 = \frac{1 - V_{p_1}^*}{2\alpha + \frac{1}{\tau^*}} \quad ,$$

and

$$C_2 = \frac{V_{p_1}^* + 1 + \frac{1}{\alpha\tau^*}}{2\alpha + \frac{1}{\tau^*}} \quad .$$

Two cases are investigated, $V_{p_1}^* = 0$, and $V_{p_1}^* = 1$, for which the constants are shown below;

	$V_{p_1}^* = 0$	$V_{p_1}^* = 1$
C_1	$\dfrac{1}{2\alpha + \frac{1}{\tau^*}}$	0
C_2	$\dfrac{1 + \frac{1}{\alpha\tau^*}}{2\alpha(1 + \frac{1}{2\alpha\tau^*})}$	$\dfrac{1}{\alpha}$

(26)

26

Presently we want to know the velocity of the particle at the exit of the tapered nozzle section, $V^*_{p_2}$. First, to find t^* at which the particle exit, we set $X^*_p = 1$ in Equation (23).

Or

$$C_1 \exp\left[-\left(\alpha + \frac{1}{\tau^*}\right)t^*\right] + C_2 \exp(\alpha t^*) = 1 + \frac{1}{\alpha} \qquad (27)$$

If $V^*_{p_1} = 1$, then $C_1 = 0$ and only the second term on the left hand side of Equation (27) is left. For small τ^*, though, the first term in Equation (27) is small in comparison with the second term and it can be neglected in a first order approximation. Hence,

$$C_2 \exp(\alpha t^*) = 1 + \frac{1}{\alpha}$$

or

$$t^*\Big|_{X^*_p = 1} = \frac{1}{\alpha} \ln\left(\frac{\alpha+1}{\alpha C_2}\right) . \qquad (28)$$

Equation (28) gives the time at which the particle reaches the exit of the tapered nozzle section.

The particle velocity is given by the derivative of Equation (23),

$$\dot{X}^*_p = \gamma_1 C_1 \exp(\gamma_1 t^*) + \gamma_2 C_2 \exp(\gamma_2 t^*). \qquad (29)$$

At $X^*_p = 1$, the particle velocity is given by substitution of equations (28) into (29),

$$\dot{X}_p^* \Bigg|_{X_p^* = 1} = V_{p_2}^* = -(\alpha + \frac{1}{\tau^*})C_1 \left(\frac{\alpha+1}{\alpha C_2}\right)^{-(1 + \frac{1}{\alpha\tau^*})} + \alpha\, C_2 \left(\frac{\alpha+1}{\alpha C_2}\right) ,$$

or

$$V_{p_2}^* = -\alpha(1 + \frac{1}{\alpha\tau^*})C_1 \left(\frac{\alpha+1}{\alpha C_2}\right)^{-(1 + \frac{1}{\alpha\tau^*})} + (\alpha+1). \tag{30}$$

Using the definition of α, Equation (20), the particle exit velocity becomes:

$$V_{p_2}^* = V_{g_2}^* - \alpha(1 + \frac{1}{\alpha\tau^*})C_1 \left(\frac{\alpha+1}{\alpha C_2}\right)^{-(1 + \frac{1}{\alpha\tau^*})} \tag{31}$$

Thus, the particle velocity at the exit is smaller than the gas velocity by a correction term given in Equation (31). If $V_{p_1}^* = 1$ then $C_1 = 0$ and the correction term is zero, making the particle velocity equal to the gas velocity all along the nozzle (to a first order approximation).

The gas velocity equation (17), can be re-arranged and written as,

$$\dot{X}_g^* - \alpha X_g^* = 1. \tag{32}$$

The BC is

$$X_g^*(0) = 0. \tag{33}$$

The solution to Equation (32) with BC (33) is,

$$X_g^* = \frac{1}{\alpha} (e^{\alpha t^*} - 1).$$ (34)

And the gas velocity is,

$$\dot{X}_g^* = e^{\alpha t^*}.$$ (35)

Or, using Equation (34), the velocity is,

$$\dot{X}_g^* = \alpha X_g^* + 1,$$ (36)

which is identical to Equation (32) or Equation (17), of a linear velocity along the nozzle (the gas velocity is exponential with time, though, as shown in Equation (35).

As a numerical example, three particle sizes are considered, 1, 10 and 15 μm. For DOP particles ρ_p = 1.1 gm/cc, the air viscosity is μ = 0.018 centipoise and the flow rate is 28.3 lit/min through each one of the jets.

Using Equation (2) and the data in Figure 4, it is found that for the first impactor stage,

$$V_{g_1} = 926 \text{ cm/sec}$$

$$S = 2.8 \text{ cm}$$

$$V_{g_2} = 2051 \text{ cm/sec}$$

Hence,

$$V_{g_2}^* = 2.215$$

and

$$\alpha = 1.215.$$

In the second stage, the only difference is

$$V_{g_2} = 9121 \text{ cm/sec}$$

or $$V_{g_2}^* = 9.85,$$

and $\alpha = 8.85$.

Table 1 summarizes the calculations based upon the substitution of the above numerical values into Equations (11), (26) and (30).

The table shows that to a first approximation, a particle entering the tapered section with a velocity equal to the gas velocity, leaves the nozzle at the same velocity as the gas. A particle which starts with zero velocity, though, comes out at a velocity approximately equal to 99 percent of the gas velocity.

Figure 7 shows the variation with time of the particle velocity, $\dot{X}_p^*$, and location X_p^* (Equations 29 and 23 respectively). The figure also shows the gas velocity, $\dot{X}_g^*$, and distance, X_g^*, as a function of time (Equations 35 and 34, respectively). The conditions in the Figure correspond to a 15 μm particle traveling in the tapered section of the nozzle of stage one, with $V_{p_1}^* = 0$. Although the time it takes the particle to travel the nozzle length is longer than the time the gas travels the same distance (time lag), the final velocities of the gas and the particle are almost identical (velocity lag). In other words, a given particle leaves the nozzle section later then a gas element — which entered the nozzle with that particle — does (particle slip).

To substantiate this claim, two approaches are taken. First the original equation of the particle velocity, Equation (15), is solved by an alternative technique (as will be shown below, this solution can not be easily integrated to yield the particle trajectory, though). And second, the equations for the straight section of the nozzle are solved. This latter approach, which does yield an exact mathematical solution to the particle behavior in a non-accelerating flow can help us to understand the particle behavior in an accelerating flow field.

30

Table 1. Calculation of Particle Velocities in the Tapered Nozzle Section

d_p, μm	τ, sec	τ^*	1st Stage						2nd Stage					
			$V^*_{p_1} = 0$			$V^*_{p_1} = 1$			$V^*_{p_1} = 0$			$V^*_{p_1} = 1$		
			c_1	c_2	$V^*_{p_2}$	c_1	c_2	$V^*_{p_2}$	c_1	c_2	$V^*_{p_2}$	c_1	c_2	$V^*_{p_2}$
1	$3.39 \cdot 10^{-6}$	$1.125 \cdot 10^{-3}$	$1.122 \cdot 10^{-3}$	0.8219	2.215	0	0.823	2.215	$1.103 \cdot 10^{-3}$	0.112	9.850	0	0.1130	9.85
10	$3.39 \cdot 10^{-4}$	$1.125 \cdot 10^{-1}$	0.0883	0.7347	2.214	0	0.823	2.215	0.0376	0.0754	9.847	0	0.1130	9.85
15	$7.64 \cdot 10^{-4}$	0.253	0.1567	0.6664	2.204	0	0.823	2.215	0.0462	0.0668	9.840	0	0.1130	9.85
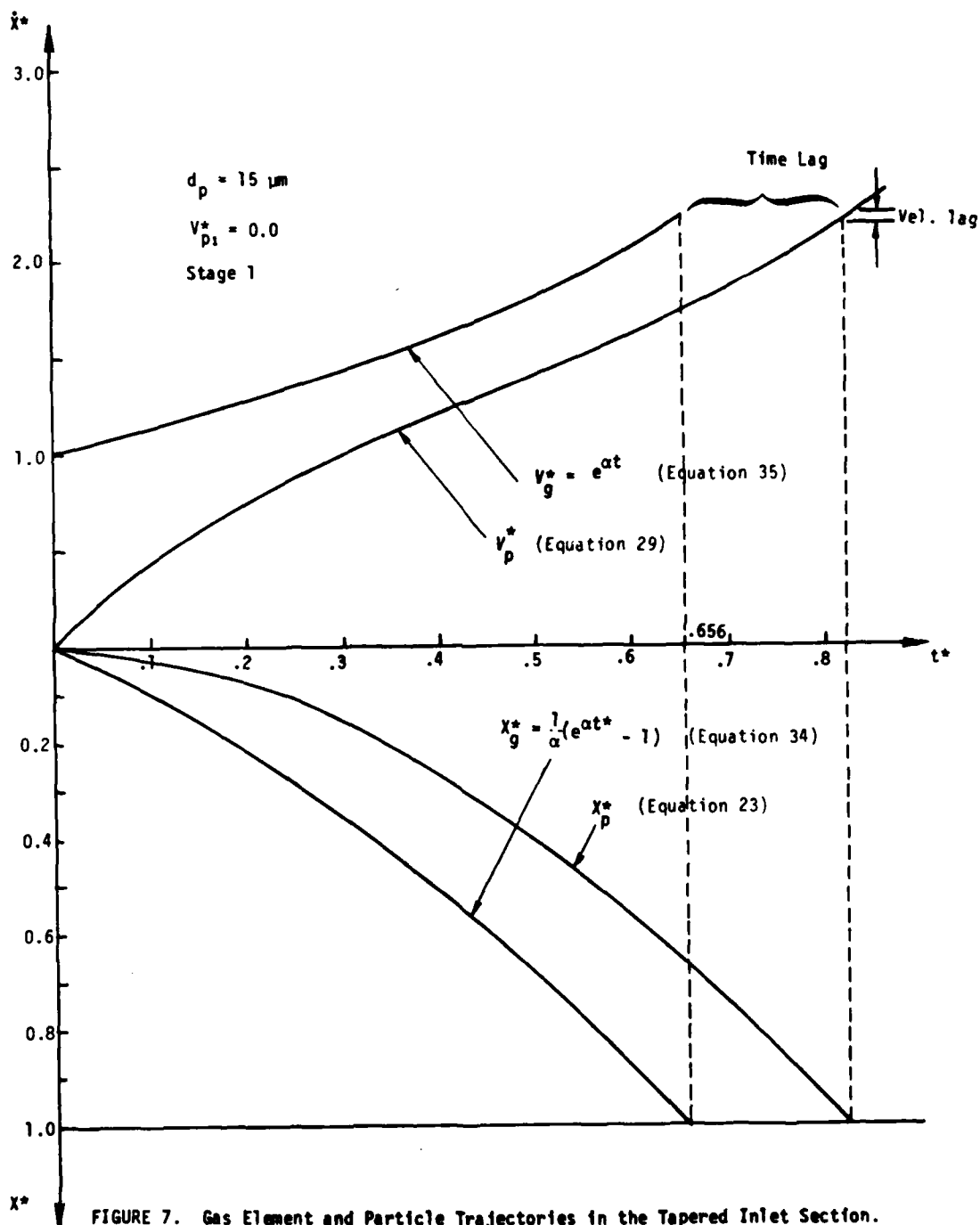
FIGURE 7. Gas Element and Particle Trajectories in the Tapered Inlet Section.

Equation (15) is solved for the velocity of a particle as a function of time for an arbitrary X. The solution is,

$$V_p = C\ e^{-t/\tau} + \frac{V_{g_1}}{\left[1-(1-\frac{D_2}{D_1})\frac{X}{S}\right]^2} \tag{37}$$

Since this solution is for an arbitrary X, it is valid for X = 0. The boundary condition at t = 0 is $V_p = V_{p_1}$.

Therefore

$$V_{p_1} = C + V_{g_1}$$

or

$$C = V_{p_1} - V_{g_1}.$$

The solution to Equation (15) is, hence,

$$V_p = (V_{p_1} - V_{g_1})\ e^{-t/\tau} + \frac{V_{g_1}}{\left[1-(1-\frac{D_2}{D_1})\frac{X}{S}\right]^2} \tag{38}$$

As already mentioned, Equation (38) can not be integrated directly to yield X_p, and hence particle flight time can not be found by this technique. For small particles, however, the characteristic time τ is very small and if the first term on the right hand side is neglected, then

$$V_p \simeq \frac{V_{g_1}}{\left[1-(1-\frac{D_2}{D_1})\frac{X}{S}\right]^2} \tag{39}$$

i.e., the particle velocity is equal to the local gas velocity. Obviously, when $(V_{p_1} - V_{g_1})$ is large, or for t values of the order of T such an approximation is invalid. Usually, however, the particles enter the

tapered section at velocities close to the gas velocity and the above solution is a good approximation to the actual situation.

2.2.2 Straight Section

In the straight section of the nozzle V_g is constant, and Equation (10) is rewritten as follows:

$$- \frac{d(V_g - V_p)}{dt} = \frac{V_g - V_p}{\tau} , \qquad (40)$$

or

$$\frac{d(V_g - V_p)}{V_g - V_p} = \frac{-dt}{\tau} .$$

In non-dimensional terms:

$$\boxed{\frac{d(1 - V_p^*)}{1 - V_p^*} = - dt^*} \qquad (41)$$

where

$$V_p^* = V_p / V_g , \text{ and } t^* = t/\tau .$$

Note that in Equation (41) the characteristic particle time τ is used to non-dimensionalize the equation (instead of $t_1 = S/V_{g_1}$ as in the tapered inlet section).

The boundary condition to this equation is the particle velocity at the inlet to the straight section (at time 0) which is equal to $V_{p_2}^*$, the exit velocity from the tapered section;

$$V_p^* (0) = V_{p_2}^* \qquad (42)$$

34

and

$$X_p^* (0) = 0.0$$

The solution to Equation (41) with B.C. (42) is,

$$V_p^* = \dot{X}_p^* = 1 - (1-V_{p_2}^*)e^{-t^*} \qquad (43)$$

Integration of this equation gives the distance the particle travels,

$$X_p^* = t^* + (1-V_{p_2}^*) (e^{-t^*}-1). \qquad (44)$$

In Figure 8, Equations (43) and (44) are plotted. This figure shows that a particle entering the straight section, for instance, at a velocity $V_{p_2}^* = 0.75$ (i.e., 75 percent of the gas velocity), takes about $t^* = 1.5$ to reach 95% of the gas velocity. By that time the particle travels a distance of $X_p^* = 1.3$. In dimensional numbers, that translates to time and distance as shown in Table 2. The second and third columns in the table show the characteristic particle time and the characteristic distance respectively. The fourth and fifth columns show the time the particle requires to reach 95% of the gas velocity and the distance it travels by that time, respectively.
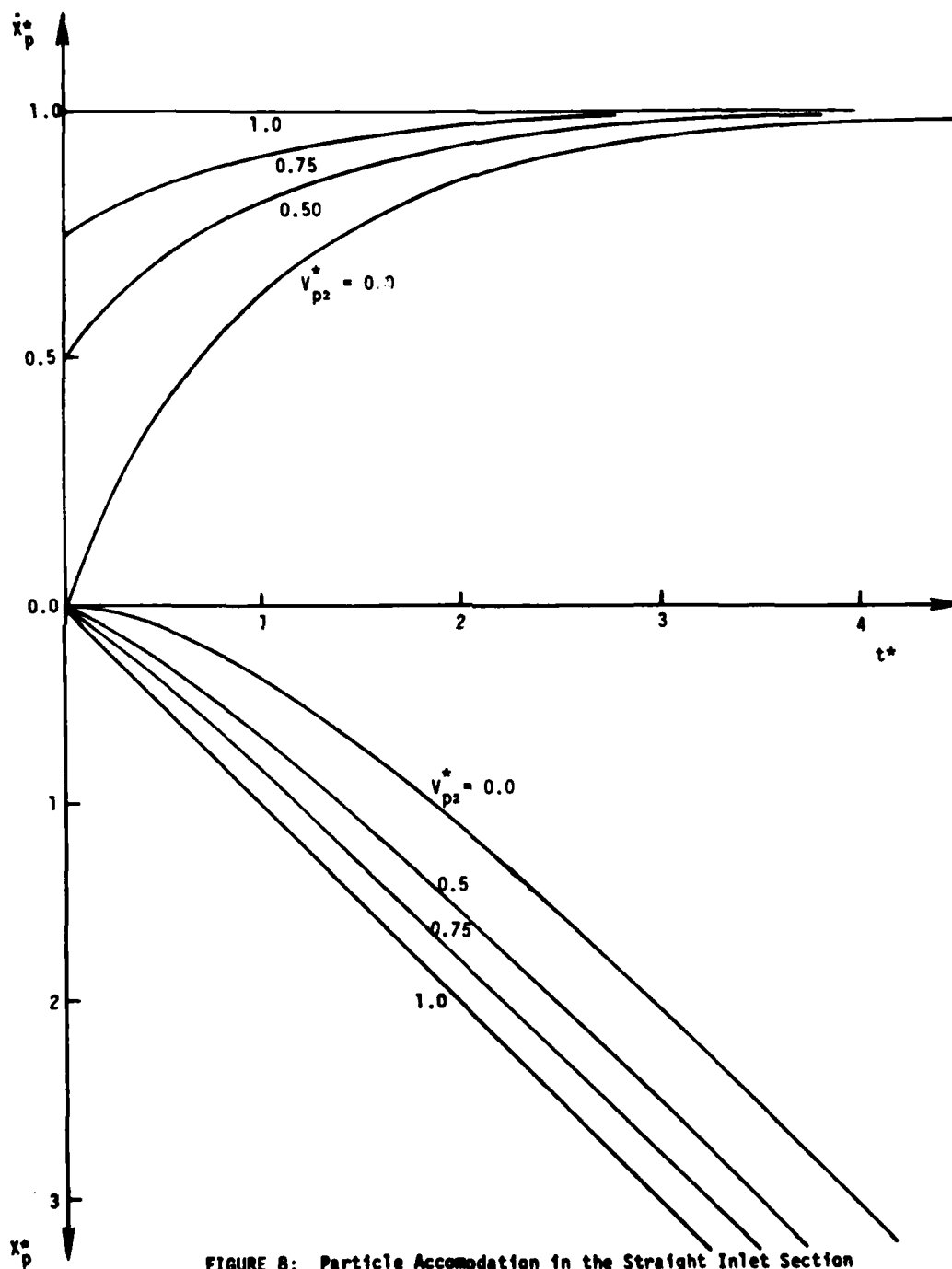
FIGURE 8: Particle Accomodation in the Straight Inlet Section

Table 2. Particle Accomodation in the Straight
Section of the Nozzle, $V_{p_2}^* = 0.75$, $V_g = 2051$ cm/sec

d_p, μm	τ, sec	$V_g\tau$, cm	$t = \tau t^*$, sec	$X_p = V_g\tau X_p^*$, cm
1	$3.39 \cdot 10^{-6}$	$6.95 \cdot 10^{-3}$	$4.41 \cdot 10^{-6}$	0.009
10	$3.39 \cdot 10^{-4}$	$6.95 \cdot 10^{-1}$	$4.41 \cdot 10^{-4}$	0.903
15	$7.54 \cdot 10^{-4}$	1.57	$1.15 \cdot 10^{-3}$	2.04

The table shows that a 15 μm particle travels a distance of
approximately 2.04 cm to accomodate to the gas velocity. It is
undesireable, however, to have a long straight section since the
boundary layer which developes in the flow creates a velocity profile
that causes a slow down of the particles close to the wall. This is
significant in particular in laminar flow, and as mentioned earlier
the nozzle may operate under such a flow condition. The conclusion
is, therefore, that the tapered section of the nozzle should be long enough
to allow almost a complete accomodation of the particles to the gas
velocity. The cone angle should not be too large so that the velocity
ratio V_{g_2}/V_{g_1} will not be large. The length of the straight section
is needed only to ensure the straightening of the particle flow in
the axial direction.

In summary, the purpose of the nozzle design is to ensure that
a polydispersed aerosol which enters the CI comes out of the nozzle with
all the particles moving at a uniform velocity. Otherwise, a small particle
may have a velocity higher than the velocity of a large particle so that

both particles leave the nozzle with the same momentum. This
situation upsets the basic principle of operation of the CI.

3. TEST SET UP AND PROCEDURES

3.1 Test Rig

A general view of the test rig is shown in figure 9. The flow control
panel shown in figure 10 and the aerosol generator in figure 11. A schematic
flow diagram is given in figure 12. The main components of the test rig
are described below, while the parts are identified in appendix A.

Shop air from a compressor is filtered and dried in a filter ① (rated
at 100% removal for 0.08 μm, and 98% removal for 0.008 μm). The air passes
through two pressure regulators ② connected in series to ensure absolute
stability of the supply pressure. The regulators are set to deliver air
at approximately 70 psig. The air enters a distribution manifold ③ and
from there it branches into three lines: one line into the aerosol generator
④ , and two lines leading into the clean side jets of the first and second
stages of the impactor, ⑤ and ⑥ . The air to the impactor stages is
metered by means of sonic orifices ⑦ and the pressure across the orifices
is monitored via a 5-way valve ⑧ and a pressure gauge ⑨ . The supply
pressure to the aerosol generator is monitored by a pressure gauge ⑩ .

A syringe pump ⑪ supplies liquid to the aerosol generator at a
preset feed rate. The liquid supply rate depends upon the pump setting
and the size of the liquid jet orifice (for details of operation of the
aerosol generator - see manufacturers specifications). To verify a uniform
feed rate, a pressure gauge and a bleed valve are connected to the drain
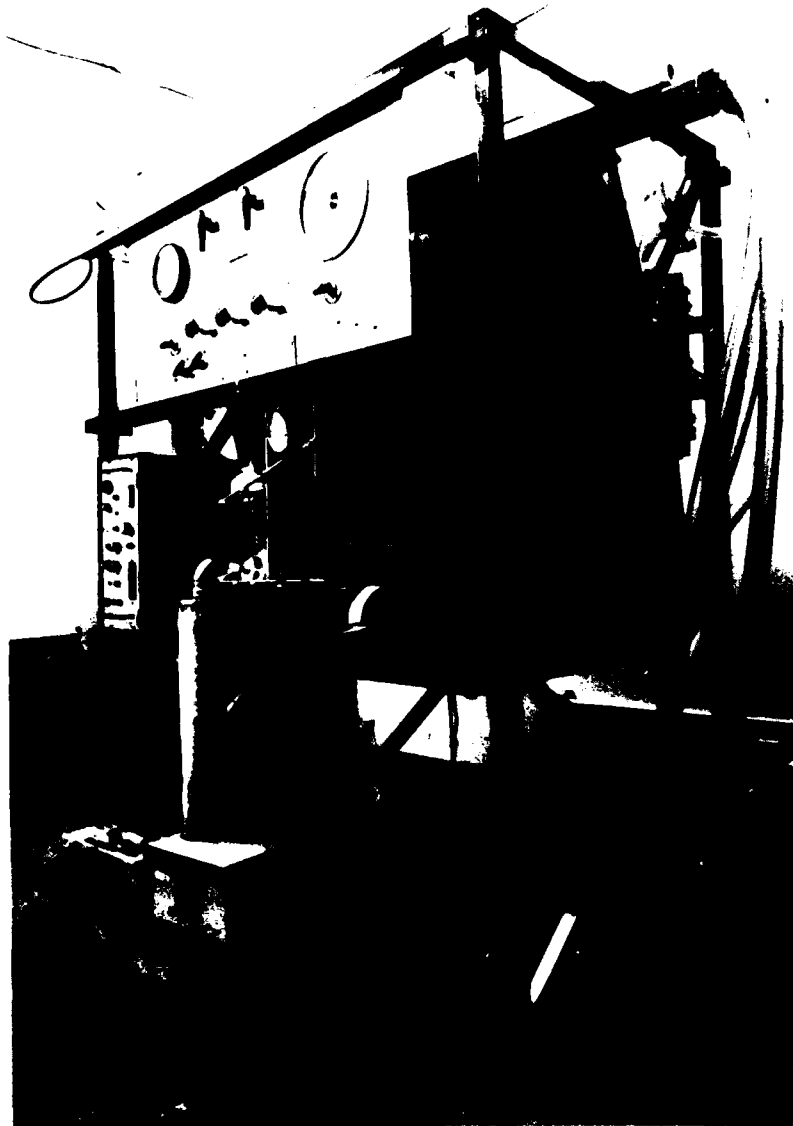
Figure 9. Continuous Impactor - Test Setup
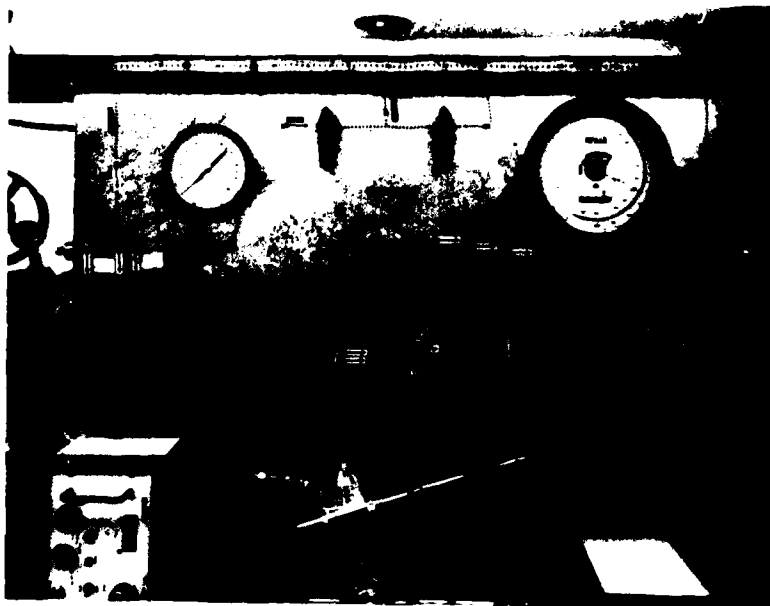
Figure 10.   Continuous Impactor - Flow Control Panel.
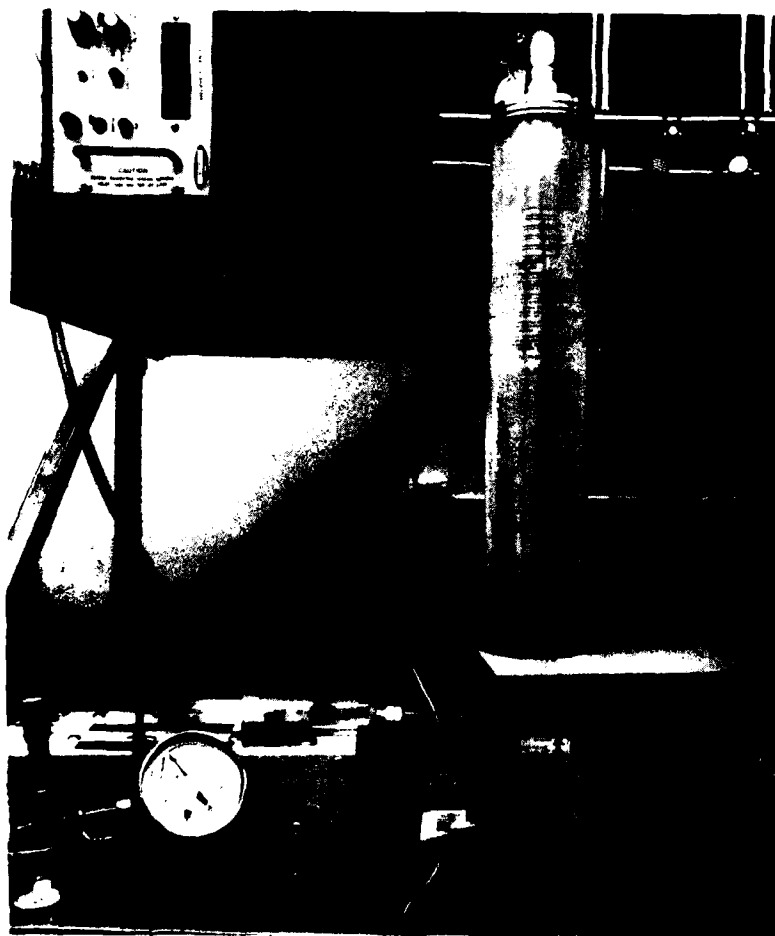
Figure 11.   Continuous Impactor - Aerosol Generator.
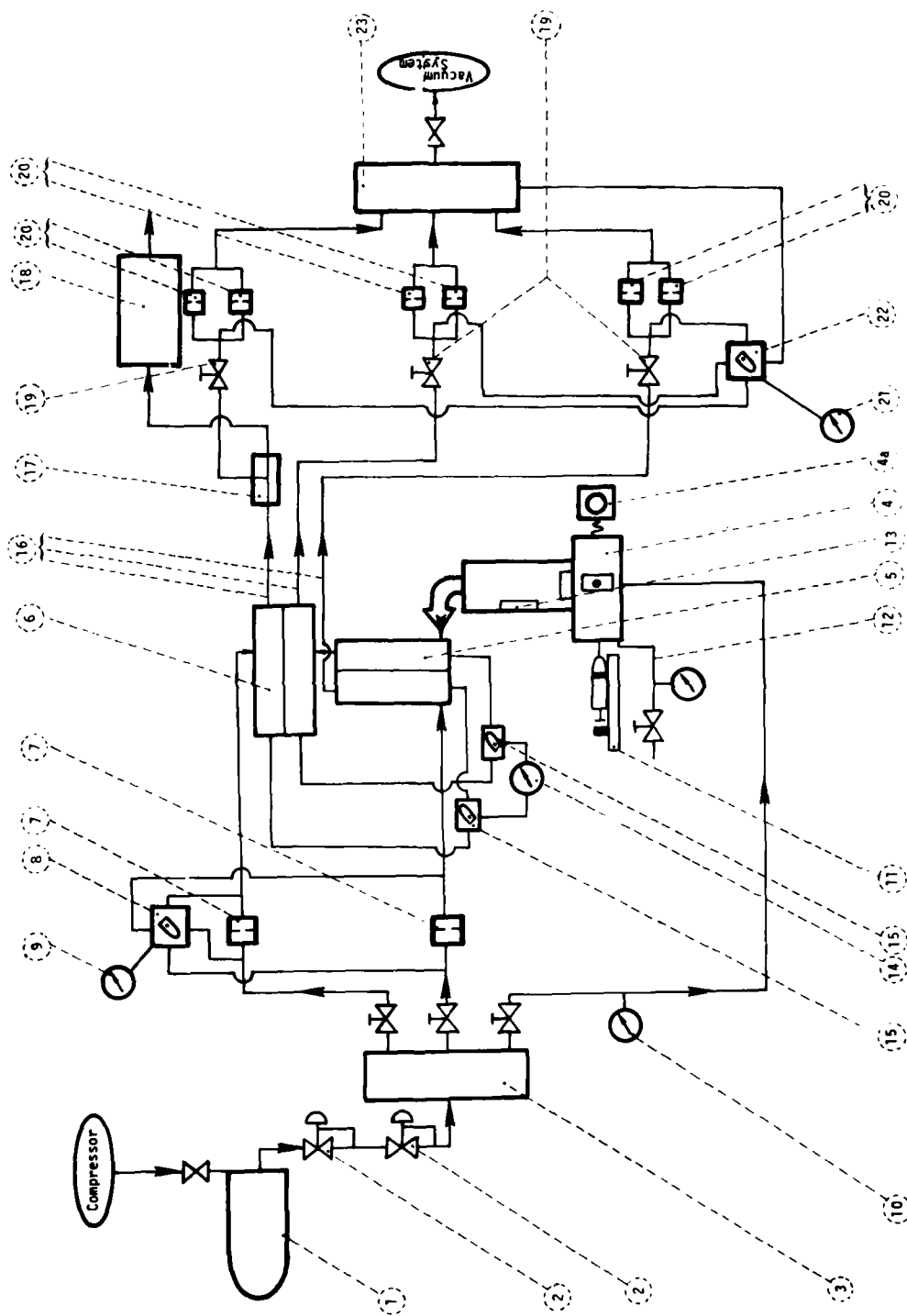
Figure 12. Continuous Impactor – Flow Diagram.

41
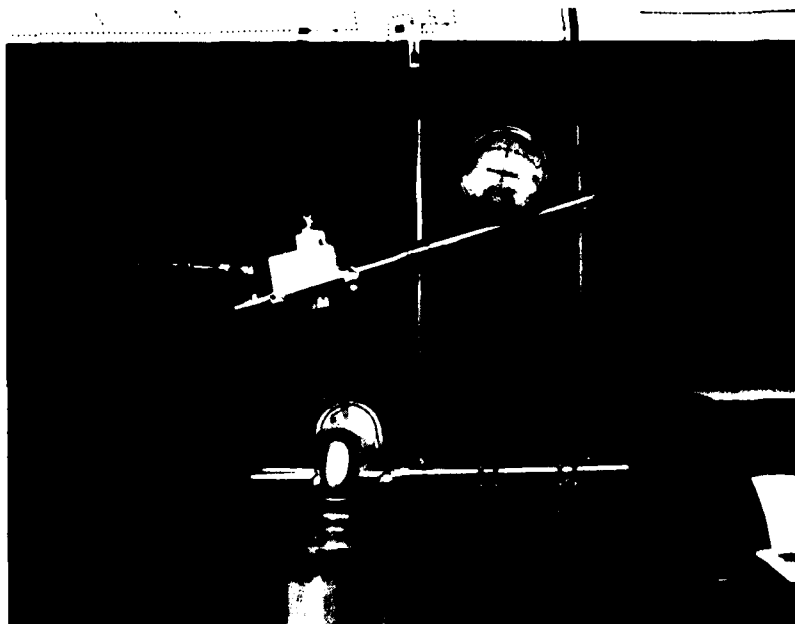
Figure 13.   Two-Stage Continuous Impactor Flow Arrangement.

3/4 SCFM to Vacuum Systems

D_1

D_2

1/4 SCFM to
Particle Counter

1 SCFM from
Impactor Stage

$L/D_2 \simeq 10$

$$\frac{D_1^2 - D_2^2}{D_2^2} \simeq 3.5$$
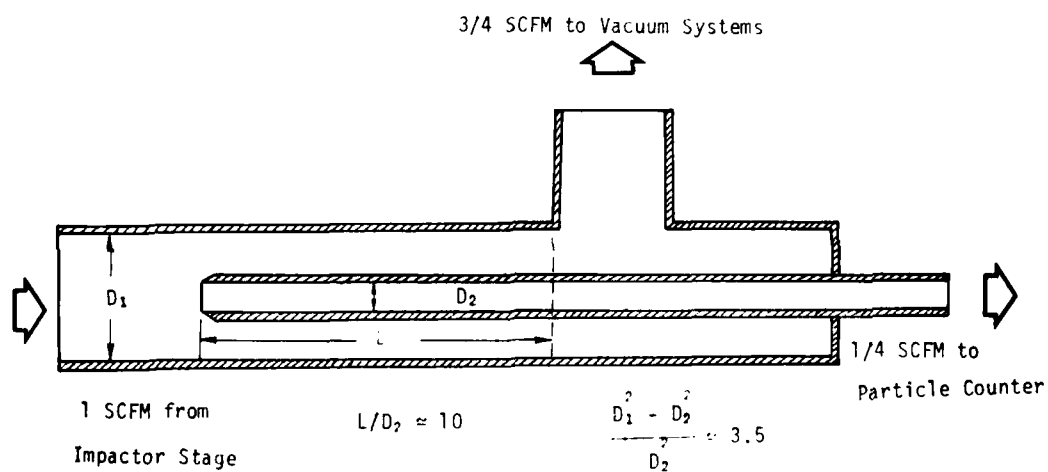
Figure 14.   Sampling Probe Design.

line ⑫ of the aerosol generator. Before entering the first impactor stage the aerosol droplets pass through a neutralizer ⑬ to remove static charge.

The two stages of the CI are set in such a way that the outlet of the first stage is connected directly to the inlet of the second stage. These details can be seen in Figure 13. The differential pressure (D/P) across each stage is monitored by a pressure gauge ⑭ , and two 3-way valves ⑮ are used to select the desired stage.

Three interchangeable exhaust lines ⑯ allow monitoring the aerosol output in each one of the streams coming out of the 2-stage CI. A specially designed sampling probe ⑰ directs one quarter of the flow of one exit line into a particle counter ⑱ . Design details of this probe are shown in Figure 14. The area ratio between the outer annulus and the inner tube of the probe is close to the ratio of the corresponding flow rates, ensuring isokinetic sampling. The sample gas is collected by the inner tube far upstream of the 90° bend in the outer flow, ensuring the collection of a representative aerosol sample. The out flow from the 2-stages of the CI is regulated by means of regulating valves ⑲ and three sets of sonic orifice fixtures ⑳ . The pressure across these fixtures is monitored on an absolute pressure gauge ㉑ by selecting the proper position of a 5-way valve ㉒ . The flow is collected in an exhaust manifold ㉓ which is connected to the building vacuum pump system (A maximum pumping capacity of over 800 CFM).

For testing of a single stage CI, the other stage is removed from the setup and its inlet and exit lines are plugged.

43

3.2 Sonic Flow Meters

Prior to the tests, all sonic orifices were calibrated by the Metrology Department. The theoretical flow equation through a sonic orifice is given by the formula,

$$SCFM = \frac{C\ FP_1}{L\sqrt{T}}\ , \qquad (45)$$

where L is the rating of the orifice in flow resistance units (see the Lee Company manual), and F is a function of the pressure ratio across the orifice. F is equal to 1 when the orifice is choked or when $P_1/P_2 \geq 0.528$ (for air). C is a constant which depends on the specific type of gas and is equal to 220 for air.

Equation (45) is rewritten as follows

$$\frac{SCFM}{P_1} = \left(\frac{C}{L\sqrt{T}}\right) F. \qquad (46)$$

Since the supply temperature is nearly constant, the quantity in the parenthesis is a constant. The left hand side of equation (46) is plotted versus a quantity which defines F, that is $1 - P_2/P_1$. For a choked orifice the theoretical curve in such a plot is horizontal.

This approach was applied to the calibration of all sonic orifices and fixtures used in the test. A sample calibration curve is shown in Appendix B.

3.3 Particle Counter

Particles are counted by the Climet CI-208 Optical Particle Counter (OPC). The instrument has six channels and a "bright-dim" switch which

44

allows changing the range of the channels. Hence, with the counter, particles can be identified as belonging to one out of twelve possible size groups (channels). These channels are listed in Table 3.

Table 3. Particle sizing capabilities of the
CI-208 OPC with a "Bright-Dim" switch

Range #	From	to	μm
1	0.3	0.5	
2	0.5	0.65	
3	0.65	1.0	
4	1.0	1.3	
5	1.3	2.3	
6	2.3	3.0	
7	3.0	5.0	
8	5.0	5.9	
9	5.9	9.5	
10	9.5	10.0	
11	10.0	20.0	
12	larger than 20.0		

A model CI-210 multichannel analyzer augments the capabilities of the CI-208 OPC. The analyzer has a switch with two ranges, each range classifying particles into one of eight channels (in addition, and independent of the CI-208 channels). The additional capabilities are summarized in Table 4 and shown schematically in Figure 15.

Table 4. CI-210 multi-channel analyzer
sizing capabilities

Channel \ Range	1			2		
	From	to	μm	From	to	μm
1	0.3	0.5		3.0	5.0	
2	0.5	0.7		5.0	8.0	
3	0.7	1.0		8.0	10.0	
4	1.0	2.0		10.0	12.0	
5	2.0	3.0		12.0	15.0	
6	3.0	5.0		15.0	17.0	
7	5.0	7.5		17.0	20.0	
8	larger than 7.5			larger than 20.0		
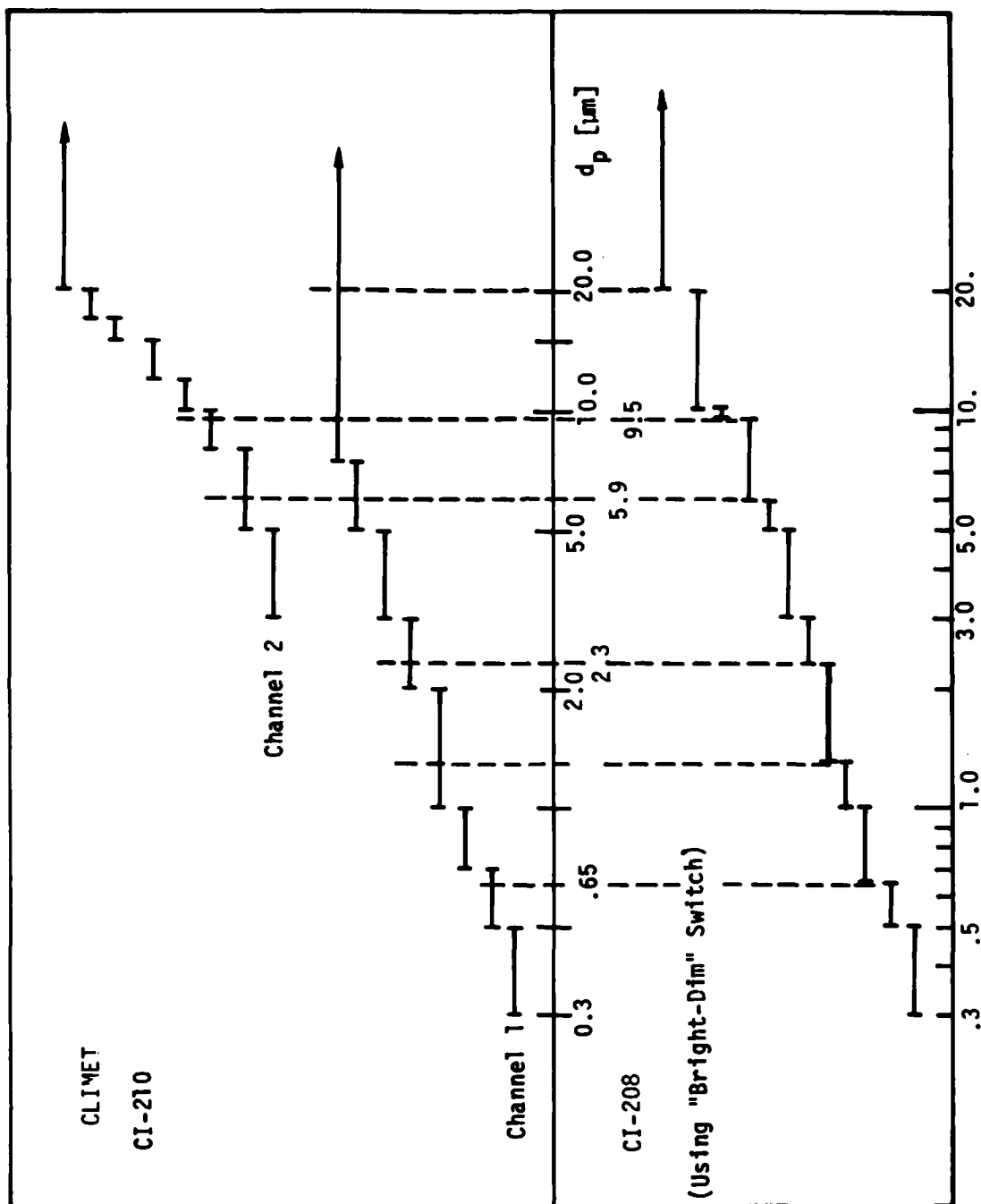
Figure 15. Particle Sizing Capabilities.

3.4 The Aerosol

The aerosol used throughout this study is made of Diocthyl-Phtalate (DOP)
liquid droplets. The technique for the generation of aerosols utilizing the
Vibrating Orifice Monodispersed Aerosol Generator (VOMAG) is discussed in
details elsewhere (Liu, 1976, and Brooks et.al, 1979).

DOP solutions in IsoPropyl Alcohol (IPA) of the following concentrations
were used; 1:8000, 1:1000, 1:500, 1:250, 1:125 and pure IPA. These solutions
and the use of a 10 and a 20 μm orifices allows the generation of particles
between approximately 0.4 to 9.0 μm. The lower limit is set by the impurities
in the IPA, and the upper limit by the excessive loss of heavy particles
in the neutrelizer column. An attempt to use a 5 μm orifice failed due to
frequent clogging of this orifice.

Another problem related to the operation of the aerosol generator is
a slow shift in the size of the generated particles. This occurs only when
the smallest particles are generated and the shift is always from small
particles to larger ones. The present explanation is that the lubricant
used in the disposable plastic syringes is slowly desolved by the IPA and
the concentration of the non-volatiles in the solution increases. Glass
syringes (type Multi fit B-D) are inadequate though, since small leaks
develop between the plunger and the cylinder.

3.5 "Noise"

To verify that the system is clean of undesired dust and free of leaks,
the test setup is operated with all parameters set to their regular operating
conditions, except the syringe pump which is left off. Under these conditions,

no particles are to be detected by the OPC. This test also confirms the cleanliness of the air supply. Frequently performed system tests have shown that no detectable particles (> 0.3 μm) or leak into the system exist other than those introduced by the VOMAG.

3.6 Performance Definition

The following definitions are adopted for measuring the performance of the Continuous Impactor.

3.6.1 Single Stage CI

- **Cross over efficiency** is the numbers of particles found in the clean jet side (side 2), divided by the sum of the particles in the clean and the aerosol sides of the CI.
  Or

$$\eta = \frac{[2]}{[2] + [1]} , \tag{47}$$

  where the following symbols are used:

  [1] - number of particles in side 1, the aerosol side.

  [2] - number of particles in side 2, the clean side.

- **Stage Particle Loss** is the difference in the number of particles entering the stage and the number leaving the stage, divided by the number of particles entering the stage.
  Or

$$L = 1 - \frac{[1] + [2]}{[I]} , \tag{48}$$

  where [I] - number of particles entering the stage.

3.6.2 2-Stage CI

- <u>Collection efficiency</u> is the ratio between the number of
  particles in the desired "window", collected through side 2
  of the second stage [2,2], and the sum of all particles
  leaving the 2-stage CI through all the exits.

  Or

  $$\eta_c = \frac{[2,2]}{[2,2] + [2,1] + [1,2]} \tag{49}$$

  where [2,1] - the number of particles leaving stage 2

  through the aerosol side ,1.

  　　　[1,2] - the number of particles leaving stage 1

  through the clean side ,2.

  and　　[2,2] - the number of particles leaving stage 2

  through the clean side, 2.

- <u>Total loss</u> is the difference between the particle input and the particle
  output of the 2-stage CI, divided by the input,

  $$L_t = 1 - \frac{[2,2] + [2,1] + [1,2]}{[I]} \tag{50}$$

It should be noted that stream [1,1], leaving stage 1 through
the aerosol side 1, is the input to the aerosol side of the
second stage.

A complete calibration curve for each stage and for the 2-stage
CI is obtained by measuring the efficiencies and losses defined above
for a number of particle sizes covering the operating range of the
CI. The tests are performed with monodispersed aerosols of a known
size.

3.7 Procedures

At the start of a test day, the particle counter is turned on, checked
and left to warm up for 50 to 60 minutes. Then, the vacuum system and the
compressed air supply are switched on. The inlet flow (clean jet side)
to each stage is set to 28.3 liters/min (std ft^3/min), and the exit flow is set to
28.3 liters/min. The exit flow in the line from which a sample is withdrawn
into the particle counter is set to 21.225 liters/min (0.75 std ft^3/min) while the
flow through the OPC is set to 7.075 liters/min (0.25 std ft^3/min). The aerosol
generator is turned on and the dilution air flow rate set at approximately
42.5 liters/min (1.5 std ft^3/min). Once the liquid feed pressure stabilizes (the
bleed valve may be used to expedite the pressure drop by allowing a small
quantity of liquid to bleed out) the droplets of a desired size are obtained.
The particle laden air, after going through the neutralizer, is directed
into the first stage inlet. Since the clean jets flow entering the two-stage
CI is metered, and the flow leaving the CI is also metered, a net flow of
28.3 liters/min (1 std ft^3/min) of aerosol-laden air is induced by suction into the
first-stage. The extra flow of aerosol-laden air is allowed to escape
around the first stage inlet. This procedure ensures that no room air
enters the CI.

Once all flow rates are set to the desired values, the differential
pressure (D/P) across the splitter plate in each stage is checked. When flows
are properly set the D/P usually does not exceed 0.5 to 1.0 inch of water
column. The final adjustment of the flow is done such that the D/P is
minimized.

Particle count is obtained for each one of the three exit lines ((16) in
figure 12) by switching the sampling probe to each of the lines. Everytime

the sampling probe is switched to another line, the flow rates and D/P
are checked and rebalanced if necessary.

The particle input to the CI is obtained by placing the sampling probe
in front of the aerosol generator. Proper care is taken to ensure that the
flow conditions at the inlet to the probe are similar to the conditions
at the inlet to the CI.

4. RESULTS AND DISCUSSION

4.1 Preliminary Test Runs

The effect of the splitter plate thickness and that of the size
of the hole in the plate upon the CI performance, was briefly investiqated.
The purpose of this investigation was to select a splitter plate which
can produce acceptable results in subsequent studies.

Initially, plates having a hole diameter two times as large as the
jet diameter (W/D = 2.0) were selected (following Brooks et al 1979). The
thickness of these plates are, in mm.: 0.0508 (2/1000"), 0.1016 (4/1000"),
0.254 (10/1000"), and 0.381 (15/1000"). It was found that the thin plates
tend to vibrate and can not be stabilized. The vibrations are
aggravated in the second stage of the CI in which the jets' velocity is
higher than the velocity in the first stage. The plate rattle produces
a high frequency sound and a very poor performance curve which stays
around 50% cross-over efficiency at all particle size.

The vibration problem practically ceased, however, for plates thicker
than 0.254 mm (10/1000"). In Appendix C, the relationship between the plate
thickness and the vibrations is shown.

Results of a few test runs with a thicker plate have not yet produced the expected performance curve. At that point the hole size in the splitter plate was changed to W/D = 1.25, following Pavlik (1978). The effect of a smaller hole is to improve cross-over efficiency but at the same time to increase losses by impaction to the plate. The reason being that the spread angle of the jets under the flow condition in the CI is very wide, and the plate surface area exposed to incoming particles increases as the hole diameter decreases.

The effect of the plate thickness on the stage particle loss has not been investigated, although Willeke and Pavlik (1979) claim to have observed such an effect. A proper design of the edge of the hole (e.g. a sharp edge) may reduce the particle loss, though.

The results discussed in the following sections were obtained for the geometry specified in Figure 4. Other parameters were fixed as follows:

- Splitter plate thickness 0.254 mm (10/1000").
- Hole diameter W/D = 1.25

The operating conditions of the jets are listed in Table 5.

TABLE 5 - CI Operating Conditions

	Stage 1	Stage 2
Flow rate, ℓ/min	28.3	28.3
Jet Reynolds number	7553	15930
Jet velocity, cm/sec	2051	9121
Nozzle diameter D, cm	0.541	0.256
Nozzle to plate spacing, ℓ/D	0.75	0.75
Nozzle length, N/D	1.0	1.0

4.2 Calibration of a Single Stage CI

The cross-over efficiency n, and the stage particle loss L, of the first and second stages, are shown in Figures 16 and 17, respectively. In order to generalize the curves for particles of various densities, the graphs are plotted as a function of the square root of the Stokes numbers, rather than the particle physical diameter, i.e.,

$$\sqrt{Stk} = \sqrt{\frac{\rho_p U}{18\mu (D/2)}} \, d_p \quad . \tag{51}$$

The particle physical diameter and the aerodynamic equivalent diameter (d_{aed}) are shown on the upper scales in each figure. This latter quantity is defined as the diameter of a particle of 1 g/cc density, that has the same terminal velocity as the actual particle (Raabe, 1976),

$$d_{aed} = \rho_p^{*\frac{1}{2}} \, d_p \quad . \tag{52}$$

The wide error bars in the figures indicate the corresponding channel in which the particle is registered by the OPC. This is done due to some uncertainty in the calculated particle size (e.g., due to small fluctuations in the liquid supply rate to the VOMAG, or possible error in the indicated frequency of the wave generator, etc.) The results of the separation efficiency and particle loss investigation in the two CI stages are discussed below. An investigation of a third stage was partially completed and the results are reported in Appendix D.
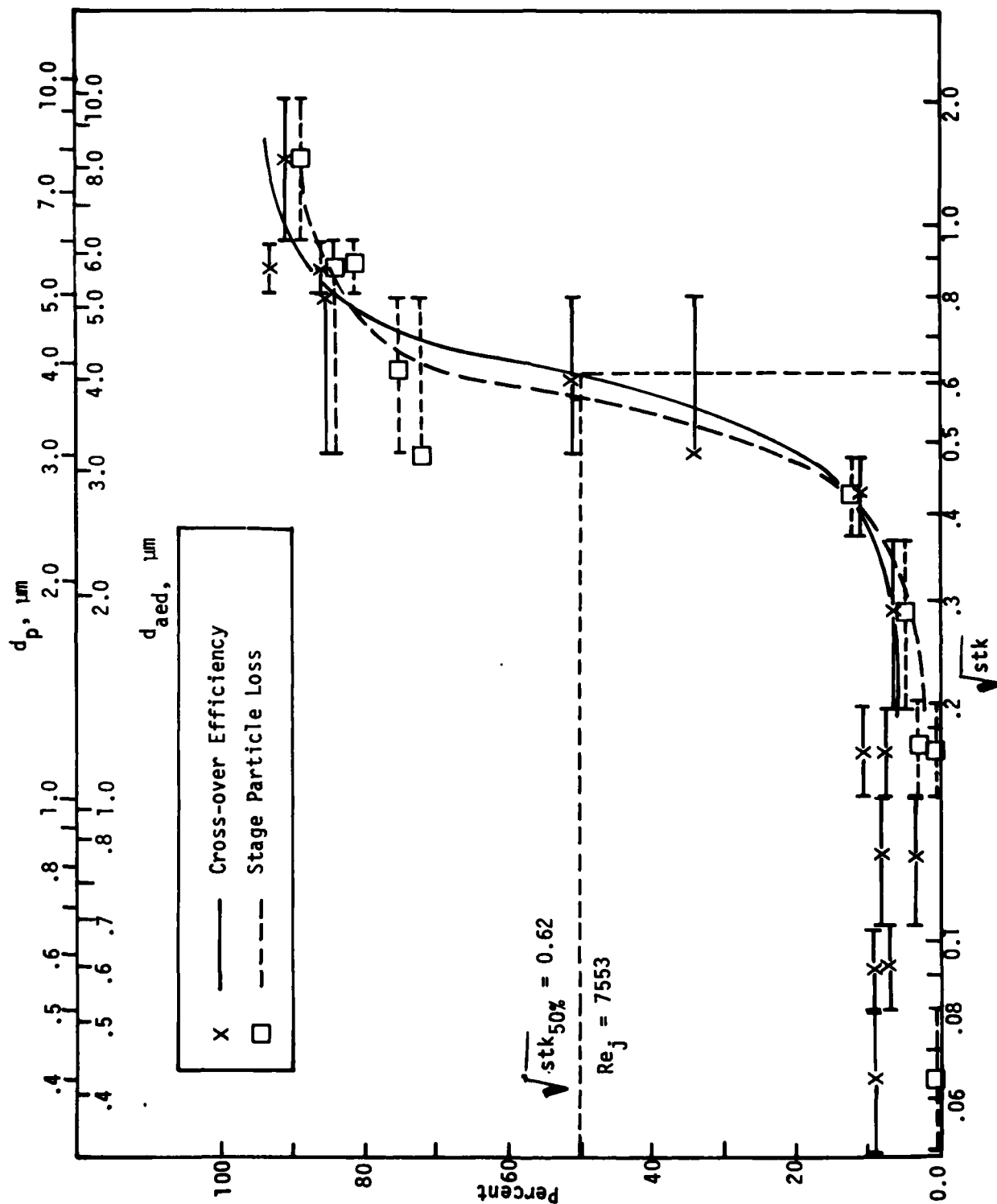
53

FIGURE 16. Performance of Stage 1 (upper scale for DOP particles)

54
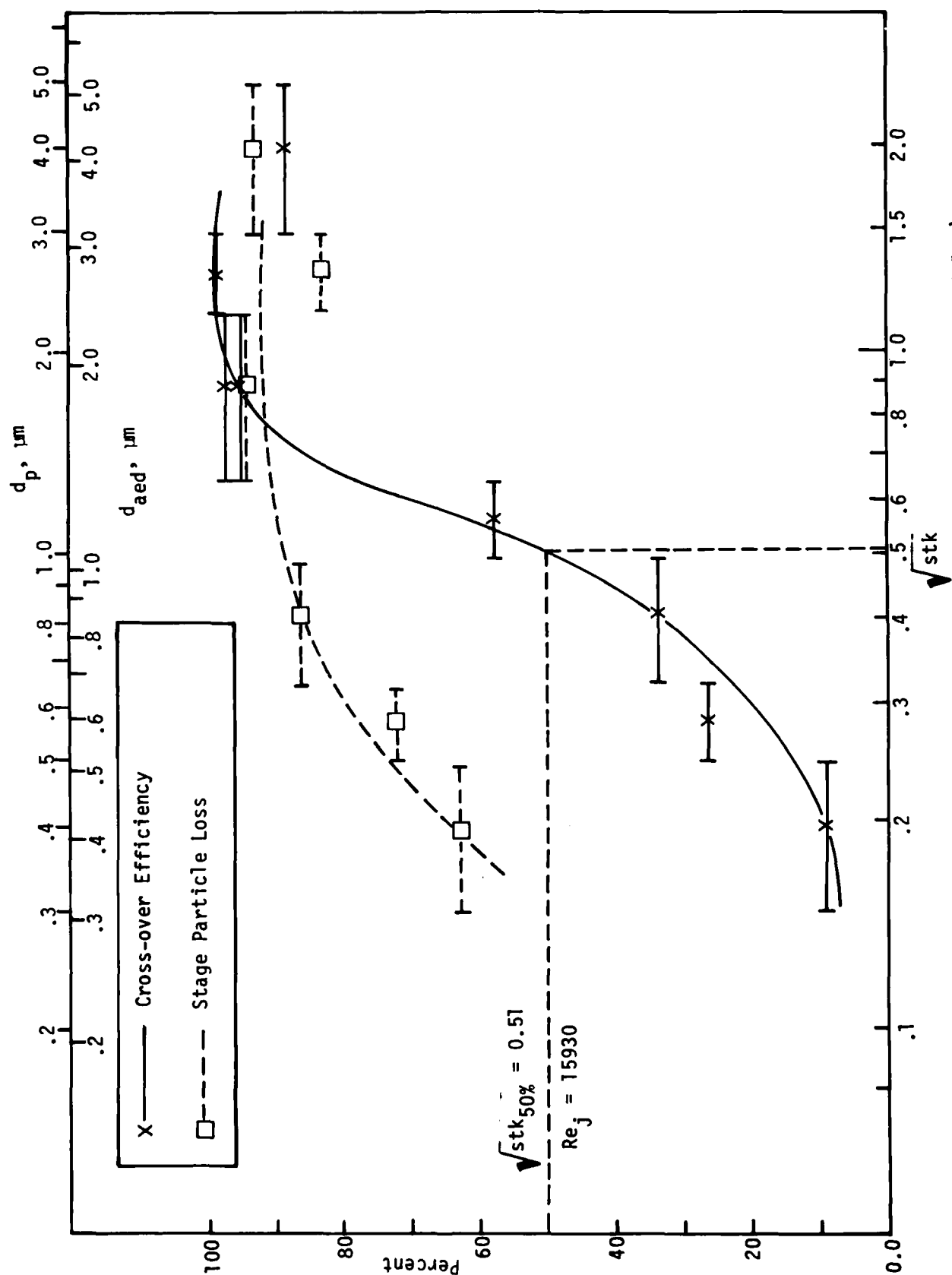
Figure 17. Performance of Stage 2 (upper scale for DOP particles)
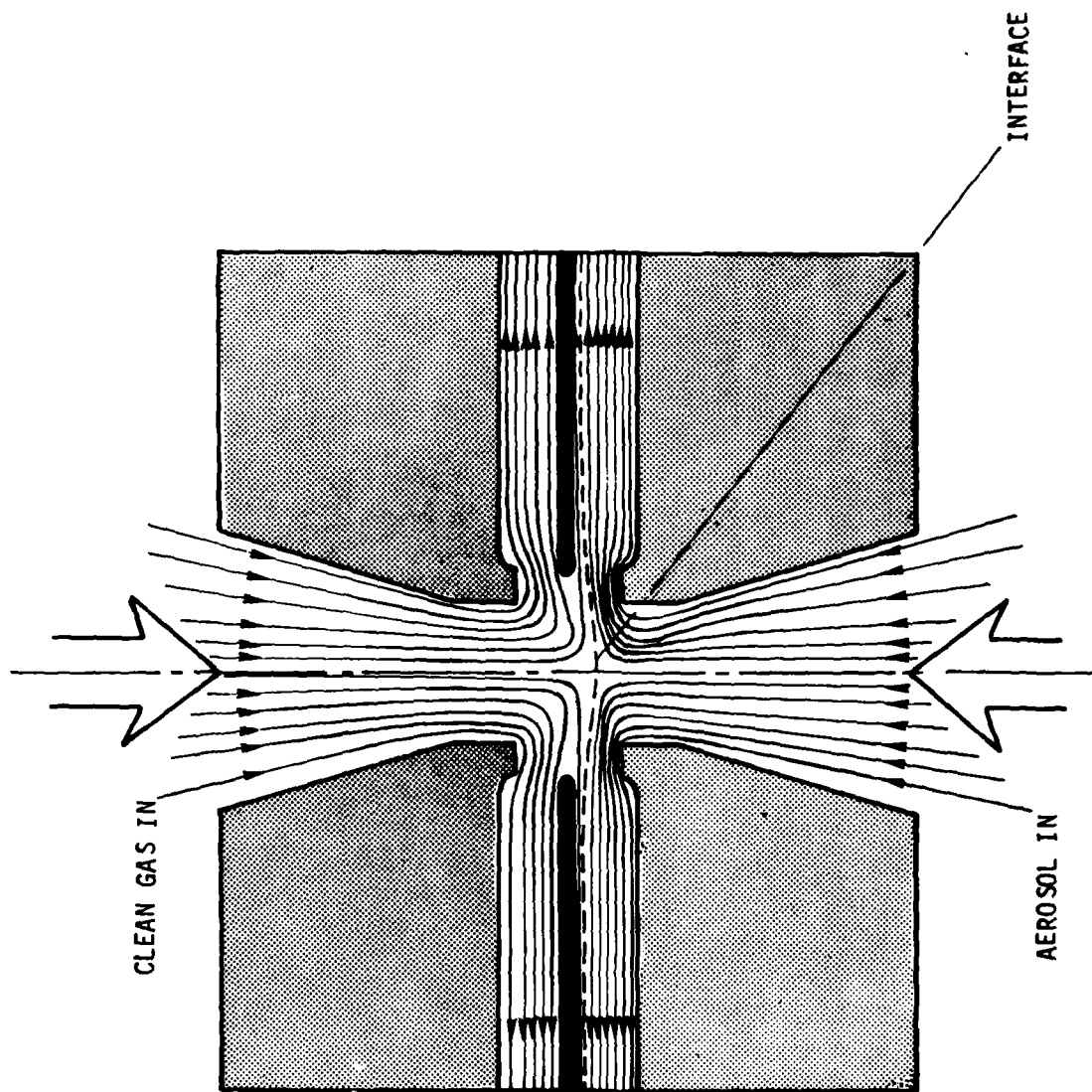
Figure 18. Imbalanced CI Operation Improves the Cross Over Efficiency for Small Particles (Note the Small Fraction of the Clean Flow Entering the Aerosol Side Collection Chamber).

4.2.1 Single Stage Separation Efficiency

The point at which the cross-over efficiency is equal to fifty percent, designated $Stk_{50\%}$, is 0.62 and 0.51 for the first and second stages respectively (or ,4 and 1 μm for DOP particles). Marple and Willeke (1976) predict values of approximately 0.46 and 0.44 according to the Reynolds numbers corresponding to the first and second stages. Their prediction is based upon an analysis of a conventional solid surface impactor, however.

A measure of the quality of the separation curve is the ratio of the particle size at 90 percent cross-over efficiency to the size at 10 percent. This parameter is approximately 2.1 and 4.0 for the first and second stages, respectively. A value of 2 would be considered a good performance for an impactor. Clearly, the second stage performance is not as good as that of the first stage. One possible reason is the high wall losses in the second stage. These losses, discussed in details below, are of such a magnitude that they are coupled to the cross-over efficiency. A decrease in the losses would definitely alter the efficiency curve of the stage.

To improve the separation efficiency there are several possible routes of investigation. First, the approximately 10 percent carry-over observed for both stages (at the small particle size range), is perhaps a result of interface instabilities which allow gas cross over from one collection chamber to the other. By setting a small imbalance in the flow of the two jets, as shown in Figure 18, it may be possible to control the small particle carry-over . The imbalance in the flow can be produced either by increasing the flow through the clean jet and reducing the flow through the aerosol laden jet by the same amount, or by increasing the exit flow on the aerosol side and reducing the exit flow on the clean side by the same amount. It

should be mentioned that a similar attempt by Brooks et al (1979) did
not produce encouraging results. Other factors could have been involved
in that experiment, however. The wisdom of this approach has to be
re-examined either experimentally or analytically. This approach opens
ways,however, to improved performance of the CI. For instance, the
fractionation point may be shifted by controlling the jets' flow. In
the extreme case in which the clean jet is completely stopped, the CI
operation becomes similar to that of the dichotomous impactor.

Another approach to improve performance of the CI is by forming a
clean gas sheath flow around the particle laden jet. The sheath which
confines the spread of the aeorsol is expected to improve the performance
of the CI. A similar approach taken by Masuda et al (1979) has proven
successful in improving the performance of a dichotomous impactor. This
was done by confining the aerosol to an annulus between a core and a
sheath flow of a clean gas. Such an approach, however, sacrifices the
simplicity of the present CI apparatus.

The reason the cross over efficiency for very large particles does
not reach a value of 100% is inherent to the operation of a CI. As
explained earlier, this occurs due to the recrossing of the interface
by heavy particles into the aerosol side after being entrained by the clean
jet, as predicted by Luna (1965). At this point it is not clear how
an imbalanced jets CI operation effects the cross-over efficiency of the
large particles.

Another reason for not reaching 100 percent efficiency is a result
of the radial distribution of particles in the jet. A particle moving in an
inner stream tube (close to the axis of the jet) encounters a flow field
different from that encountered by a particle moving in an outer stream tube.
While the former may have a sufficient momentum to cross over, the latter may

58

be deflected by the flow and stay in the aerosol side. The reason being
that the latter particle has to cross a large volume of deflected flow
before reaching the interface.

In the next section it is shown that the distribution of particles
in the jet may lead to part of the losses in the CI.

4.2.2 Single Stage Particle Loss

The stage particle loss is relatively low for particles under the 50 percent
fractionation point and the loss is high above that point in the first
stage. This is not untypical behavior for impactors of all kinds (Willeke
and Pavlik, 1978; Loo et al, 1973), although in some cases losses are
high only around the fractionation point and low on both sides of that
point. In the second stage particle loss is high through out the range
of operation.

Qualitatively, wall losses were investigated by visual observations.
Surfaces inside the CI on which particles impact are usually wet and easily
identifiable as cirtical areas. It was observed that most of the losses
occur on the splitter plate in an annulus around the center hole, mainly on
the side facing the aerosol jet. The accumulated "wetness" is high close
to the hole and it decreases with the radial distance away from the hole. All
the "wetness" is confined to an area of approximately three times the jet
diameter. No asymmetry in the particle deposition is observed (as would
be expected due to the oblong shape of the chambers).

The reason for the losses in this area is related to the radial
distribution of the particles in the nozzle. This relation is particularly
pronounced for particle sizes around the 50% fractionation point. While
particles close to the axis of the jet cross over to the clean side, and the
particles close to the perimeter of the jet are deflected by the flow, some
particles at intermediate radial locations may impact on the plate.

59

If all particles are much smaller or much larger then the 50 percent fractionation point, this explanation is not satisfactory, though, and other loss mechanisms are to be suspected.

A "wetness" pattern, similar to that found on the side of the splitter plate facing the aerosol, is observed on the other side of that plate. This can be attributed to particles which cross over to the clean side, propagate some distance upstream the clean jet and eventually reverse their flow direction. Those particles behave as if they entered the CI with the clean jet (albeit at a velocity smaller then that of the jet), and some may impact on the splitter plate due to the same reasons that this occurs on the aerosol side.

Another surface on which particles are accumulated is an annulus around the jet exit, both on the clean and on the aerosol side of the CI. These losses are related to particle trajectories, in particular of a very heavy particle. Re-design of the nozzle exit (e.g., recessing the walls around the jet nozzle) may reduce these types of losses.

The loss to the splitter plate can not be easily eliminated. If the hole in the plate is enlarged, interface instabilities may become detrimental to the cross-over efficiency. Thus it is a problem of optimizing the loss versus the efficiency.

No other surfaces of significant particle loss were identified.

4.3 Calibration of a 2-Stage CI

Once the calibration of the separate stages is completed, the
second stage is connected to the first one in such a way that the
fraction of the small particles leaving stage one enters stage two for
further fractionation. The fraction of the large particles leaving stage
two is, therefore, in a "window" size range between the fractionation
points of the two stages.

Based upon the calibration of the two separate stages, a prediction
of the combined 2-stage performance is obtained as follows.
The subscripts 1 and 2 refer to loss and efficiency in the corresponding stages:

- The fraction of particles lost in stage one is,

    L_1

- The fraction of particles leaving stage 1 through side 2, [1,2] is

    $(1 - L_1) \, \eta_1$

- The fraction of particles leaving stage 1 through side 1, [1,1] is

    $(1 - L_1) \, (1 - \eta_1)$.

- This is also the fraction of particles entering stage 2.

- Next, the fraction lost in stage 2 is,

    $L_2 \, (1 - L_1) \, (1 - \eta_1)$.

- The fraction leaving stage 2 through side 2, [2,2],

    $\eta_2 \, (1 - L_2) \, (1 - L_1) \, (1 - \eta_1)$.

- The fraction leaving stage 2 through side 1, [2,1],

    $(1 - \eta_2) \, (1 - L_2) \, (1 - L_1) \, (1 - \eta_1)$.

By definition of the collection efficiency, and the total particle
loss, equations (49) and (50), the following expressions are obtained:

$$\eta_c = \frac{(1-L_2)\ (1-L_1)\ (1-\eta_1)\ \eta_2}{(1-L_1)\ \eta_1 + (1-L_1)\ (1-L_2)\ (1-\eta_1)\ \eta_2 + (1-L_1)\ (1-L_2)\ (1-\eta_1)\ (1-\eta_2)} \cdot \quad (53.$$

Or after some re-arrangement,

$$\eta_c = \frac{(1-L_2)\ (1-\eta_1)\ \eta_2}{1-L_2\ (1-\eta_1)} \cdot \qquad\qquad (54)$$

Equation (54) shows that the collection efficiency does not depend upon the loss in stage one, L_1. It does depend, though, upon the loss in stage two, L_2. This result is obtained since the loss in stage one is implicitly assumed to be equally divided between the two leaving streams. In this case the term $(1-L_1)$ cancels out from the equation. This assumption is necessary since the loss is accounted for as an integral quantity characteristic to the stage, and it can not be separately measured (at the present time) for each side of stage one. In reality particle loss in the aerosol side is not necessarily equal to that in the clean side.

The maximum theoretical efficiency achieved when $L_2 = 0$, is

$$\max \eta_c = (1 - \eta_1)\ \eta_2 \cdot \qquad\qquad (55)$$

The total loss in the combined 2-stage CI is the sum of the individual losses,

$$L_t = L_1 + (1 - L_1)\ (1 - \eta_1)\ L_2 \cdot \qquad\qquad (56)$$

Using the above formulae, and the calibration data of the two stages, a predicted collection efficiency curve and a predicted total loss curve are calculated and plotted in Figure 19. Also shown in the figure, are the experimental data taken on the 2-stage CI. The general trend of the predicted curve is confirmed in spite of some scatter in the data.

An ideal "window" would be rectangular in shape, and it corresponds to individual efficiency curves of a step function form with no stage losses. The observed "window" in the present test is less than ideal. Particularly undesirable are the long tails on both sides of the window. To eliminate these tails, it is necessary to improve each stage efficiency and reduce the stage particle loss as discussed earlier.

Finally, attention should be given to the operation of the CI with solid particles as opposed to liquid droplets used in the present study. Pavlik (1978) has shown that stage particle loss is smaller for solid particles. The reason is that solid particles bounce off the walls and essentially remain in the flow. Under these conditions the cross over efficiency may change as well. No experimental work was done in the present investigation to verify this claim.
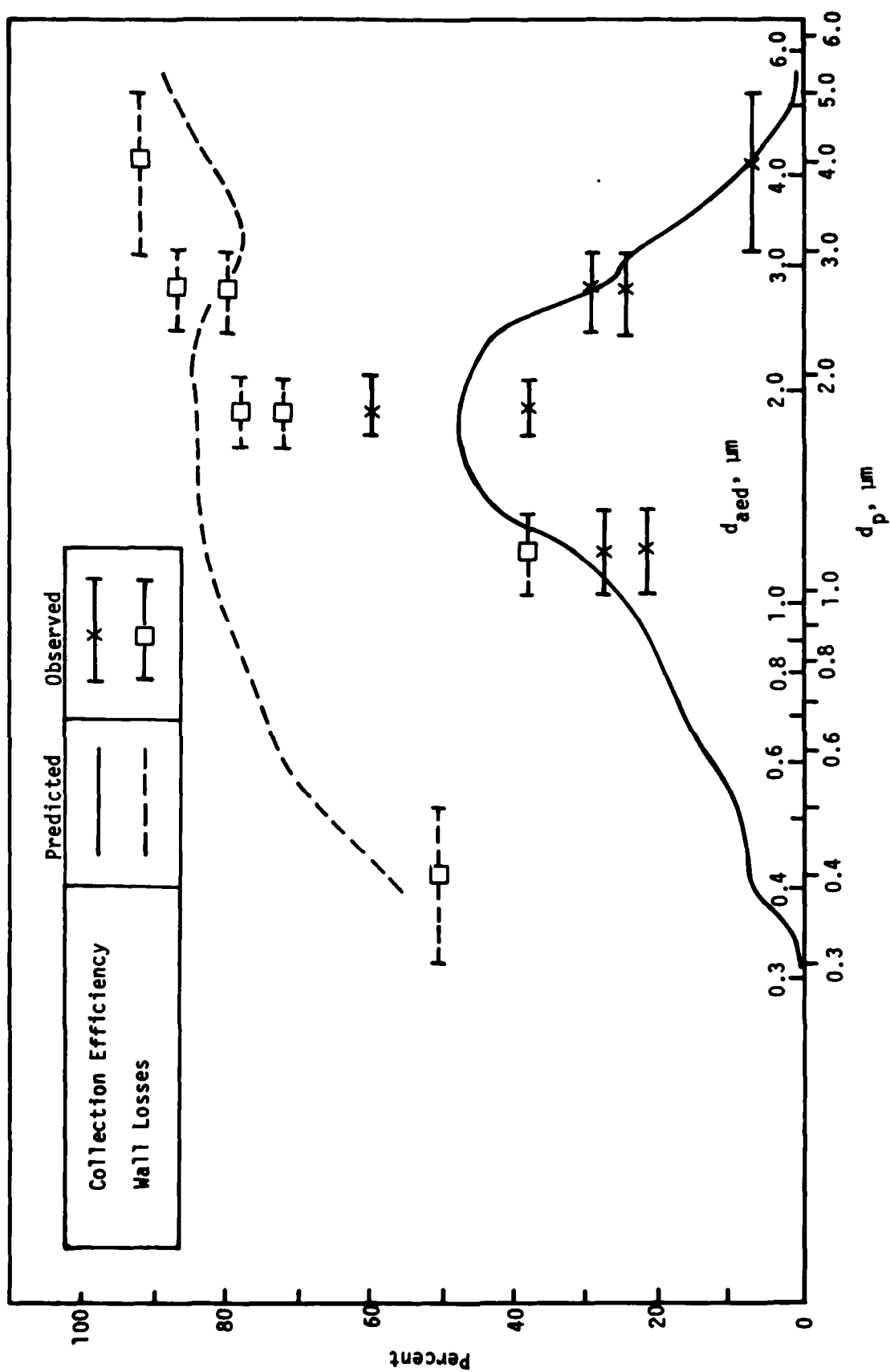
Figure 19. 2-Stage CI Performance Curves

4.4 Notes on the Status and Potential of the CI

In the last few years several manufacturers entered the market with a single stage dichotomous samplers (Beckman Inst, Andersen, Sierra) which are designed to fractionate particulates at approximately 2.5μm. A preseparator installed on the inlet removes aprticulates larger than 15μm. Such samplers are usually built for automated sampling over an extended period of time.

In comparison to these dichotomous samplers, the CI is still not mature for immediate application. However, the information and knowledge gained through recent studies (Luna, 1965; Brooks et al, 1979, Pavlik, 1978; and the present investigation) points out to several advantages of the CI which make it an attractive instrument. First, it is shown that the concept of an opposed jet sampler can be applied in practice and that the CI can perform as well as a comparable single stage impactor. Also the present study has indicated that a cascaded CI is possible. The idea can be developed into a cascade sampling probe for the collection of aerosols in several "windows". Such a probe may have applications for sampling of stationary (stacks) and mobile sources (automobile exhaust), or of ambient air at heavy smoke concentrations. In addition, the CI is very flexible to operate, and its fractionation points can be shifted by means of flow control.

Another potential application of the CI is, for instance, in the generation of monodispersed aerosols. By collecting polydispersed aerosol of a similar density and passing it through the CI, an output of monodispersed aerosol in a desired size range is obtained. Further, the 2-stage CI can be used to measure densities of spherical particles by passing the particles leaving the CI through an OPC. The OPC measures

65

the particle physical diameter, and the density is calculated from the aerodynamic equivalent diameter (or Stokes number). In the case of non-spherical particles of a known density, the CI can be used to estimate the shape factor of particles of a known aerodynamic equivalent diameter.

As indicated above, though, the CI is not ready yet for an immediate laboratory use or for commercialization. There are several areas in which an additional study and analysis is needed in order to bring about the required improvements in the performance of the CI. One aspect of the development of the CI in which insufficient progress has been made to date is the development of an analytical model. The importance of such an analytical s dy is underscored by the contribution made by Marple's (1970) analysis to the development of conventional impactors.

The first task is, therefore, the definition of the scaling laws of the CI and the generation of an analytical data base. This task requires the modeling of the flow field in the space confined by the nozzles' exit and the collection chambers' wall. A similar approach with various degrees of complication can be found in the literature. For a solid wall impactor, for instance, Ranz and Wong (1952) used simplified (potential flow) equations for the flow field approximation. Marple (1970) solved the full Navier-Stokes equations including the viscous terms (incompressible) throughout the flow field. For impinging jets type impactor, Luna (1965) approached the problem by solving the inviscid imcompressible flow equations.

To improve the results of the aforementioned studies it may be necessary to take into account viscosity (in particular in the interface zone between the two jets) and the non-symmetry of the apparatus. The analytical effort should be supported by some flow visualization studies done on a transparent CI model. In addition to a data base, the better

66

understanding of the particle behavior in the CI – a direct outcome of
the modelling study – should lead the required hardware modification.
The next step should be recalibration of the apparatus utilizing solid
particles as well as liquid droplets. Furthermore, the CI should be
operated at off design conditions (e.g. at various flow rates) and the
corresponding shifts in the calibration curve identified. Finally,
the CI should be tested under real field conditions and various realistic
requirements.

5. SUMMARY OF RESULTS

1. The oblong shape of the collection chambers and the location of the exit ports in the chambers practically eliminate the problem associated with the non-symmetry of the apparatus. This is an improvement over the first model's circular chamber.

2. With the present collection chamber design the thickness of the splitter plate has to be at least 0.254 mm (10/1000") to eliminate vibrations.

3. The splitter plate vibrations are more pronounced in the second stage in which the jets' velocity is higher.

4. The $\sqrt{Stk_{50\%}}$ is 0.62 and 0.51 for the first and second stages respectively. The corresponding Reynolds numbers are 7553 and 15930.

5. The cross over efficiency steepness parameter (defined as d_p @ 90% cross over efficiency divided by d_p @ 10% cross over efficiency) is 2.1 and 4 for the 1st and 2nd stages, respectively. A value of 2 is considered as good performance for solid wall impactors. The relatively poor performance of the second stage is attributed to the high particle loss in that stage as well as to the small particle carry over. The latter may be eliminated by a small over flow on the clean jet side.

6. Two major sources of particle loss by impaction have been identified. Impaction around the jet nozzle exit may be reduced by recessing of the chamber faces. Impaction on the splitter plate has to be optimized with respect to the separation efficiency by controlling the hole diameter in the plate (loss minimization and separation efficiency are inversely related).

7. Particle loss around the 50% fractionation point size is inherent to the operation of the CI due to the radial distribution of particles in the jet, but may be minimized by the use of a clean air sheath.

8. The performance of the two-stage CI follows the expectations based upon the performance of the individual stages. The apparatus delivers aerosol in a window between 1 to 4 µm (DOP Particles). The peak collection efficiency in that window is around 50% and it has two undesired "tails". A reduction in the stage particle loss and an improved efficiency is needed to increase the peak collection efficiency and cut the "tails".

6. RECOMMENDATIONS FOR FUTURE WORK

The following tasks recommended for a future work on the optimization of the CI performance are a logical follow up to the present investigation. Although other routes may be taken, these tasks seem to provide a rational and cost effective approach to tackle the deficiencies identified in the present investigation. So far, the development of the CI has proceeded along a craftsmanship course with some minimal engineering interjection. Therefore, the tasks listed below - directed toward the goal of the development of an optimal CI for field and laboratory application - make use of advanced engineering research and development techniques.

- A detailed anlaytical model of the flow field inside the impactor, in particular the viscous interface between the two jets, is to be established.

- A theoretical performance data base, generated by means of numerical techniques, is to be used for the identification of hardware performance problems.

- Flow field visualization, a powerful tool in many fluid dynamics studies, is recommended as an aid for the modeling task.

- Recessing the collection chamber faces and other minor geometrical modifications (to be identified by the analytical model) are required to reduce wall losses.

- An optimization of impaction losses on the splitter plate versus the separation efficiency has to be performed in order to identify the "best" hole size in the plate.

- A complete mapping of the CI performance has to be performed. This task includes calibration at various flow rates utilizing both solid and liquid particles.

REFERENCES

Austin, T. M. (1979). "Techniques for Particle Measurement." Industrial Research and Development, Feb. 1979, pp. 129-132.

Baumeister, T. Editor, (1976). "Mark's Standard Handbook for Mechanical Engineers." Seventh Edition, The McGraw-Hill Book Company.

Brooks, E. F. et al (1979). "Development Study of a Novel Continuous Flow Impactor". EPA-600/7-8-014, January 1980.

Conners, W. D. (1966). "An Inertial-Type Particle Separator for Collecting Large Samples. " J. of the Air Pollution Control Association, Vol. 16, No. 1, January, pp. 35-38.

Dzubay, T. G., and Stevens, R. K. (1975). "Ambient Air Analysis with Dichotomous Sampler and X-ray Fluorescence Spectrometer." Environmental Science & Technology, Vol. 9, No. 7, pp. 663-668.

Hall, R. E. (1970). "Axisymmetric Impinging Jet Flows and Their Application to Particle Size Classification." M. S. Thesis, the University of Kentucky.

Hounam, R. F., and Sherwood, R. J. (1965). "The Cascade Centripeter: A Device for Determining the Concentration and Size Distribution of Aerosols." Industrial Hygiene Journal, March-April, pp. 122-131.

Lapple, C. E. (1968). "Particle Size Analysis and Analyzers." Chemical Engineering, May 20, pp. 149-156.

Lee, R. J., Fasiska, E. J., Janocko, P., McFarland, D., and Penkala, S. (1979). "Electron-Beam Particulate Analysis." Industrial Research and Development, June 1979, pp. 105-108.

Liu, B. Y. H. (1976). "Standardization and Calibration of Aerosol Instruments." Fine Particles, Aerosol Generation, Measurement, Sampling, and Analysis, Liu, B. Y. H. (Editor), Academic Press Inc, pp. 39-53.

Loo, B. W., and Jaklevic, J. M. (1973). "An Evaluation of the ERC Virtual Impactor." Lawrence Berkeley Laboratory Report No. LBL-2468.

Loo, B. W., Jaklevic, J. M., and Gouldin, F. S. (1976). "Dichotomous Virtual Impactors for Large Scale Monitoring of Airborne Particulate Matter." Fine Particles, Aerosol Generation, Measurements, Sampling and Analysis, Liu, B. Y. H. (Editor), Academic Press Inc. pp. 311-350.

Luna, R. E. (1965). "A Study of Impinging Axisymmetric Jets and Their Application to Size Classification of Small Particles." PhD Dissertation, Princeton University.

Marple, V. A. (1970). "A Fundamental Study of Inertial Impactors." PhD Dissertation, The University of Minnesota.

Marple, V. A., and Willeke, K. (1976). "Inertial Impactors: Theory, Design and Use." Fine Particles, Aerosol Generation, Measurement, Sampling and Analysis, Liu, B. Y. H. (Editor), Academic Press Inc., pp. 411-446.

Masuda, H., Hochrainer, D., and Stober, W.(1979). "An Improved Virtual Impactor for Particle Classification and Generation of Test Aerosols with Narrow Size Distribution." Journal of Aerosol Sciences, Vol. 10, pp. 275-287.

McFarland, A. R., Ortiz, C. A., and Bertch, R. W. (1978). "Particle Collection Characteristics of a Single Stage Dichotomous Sampler." Environmental Science and Technology, Vol. 12, No. 6, June, pp. 679-682.

Mears, C. E. (1973). "Two Dimensional Impinging Jet Flows and Their Application to Particle Size Classification." M. S. Thesis, the University of Kentucky.

Pavlik, R. E. (1978). "Size Classification of Fine Particles by Axisymmetric Opposed Air Jets." PhD Dissertation, the University of Cincinnati.

Raabe, O. G. (1976)."Aerosol Aerodynamic Size Conventions for Inertial Sampler Calibration." J. of the Air Pollution Control Association, Vol. 26, No. 9, September pp. 856-860.

Ranz, W. E. and Wong, J. B. 1952, "Impaction of Dust and Smoke Particles". Industrial and Engineering Chemistry, Volume 44, No. 6, pp. 1371-1381.

Schlichting, H. (1968). "Boundary Layer Theory." The McGraw-Hill Book Co., Sixth Edition, p. 37.

Torobin, L. B., and Gauvin, W. H. (1959). "Fundamental Aspects of Solid-Gas Flow; Part I, Introductory Concepts and Idealized Sphere Motion in Viscous Regime." The Canadian Journal of Chemical Engineering, August, pp. 129-141.

Willeke, K., and Pavlik, R. E. (1978). "Size Classification of Fine Particles by Opposing Jets." Environmental Science & Technology, Vol. 12, No. 5, May, pp. 563-566.

Willeke, K., and Pavlik, R. E. (1979). "Secondary Effects in Particle Size Classification by Opposing Jets." Journal of Aerosol Sciences, Vol. 10, pp. 1-10.

APPENDIX A

Test rig parts list and manufacturers.

1. Air Products and Chemicals, filter housing (part #E40-8-16441) and a CV Petrosorb Ultipore disposable filter element (#E40-Q-18162).

2. Moore Products Co., 0-100 Psig, high flow pressure regulator (#40H100).

3. Home made 1" manifold.

4. TSI Model 3050 Vibrating Orifice Monodispersed Aerosol Generator, (Berglund-Liu).

4a. B&K Precision, Division of Dynascan Corporation, Model E3108 wave generator.

5 & 6 Home made, CI stages one and two.

7. The Lee Company, Lee Jet in Fitting (#JETB1872850L).

8. Swagelok, 5-way ball valve (#B-43ZF2).

9. Matheson Gas Products, 0-100 Psig, 0.25% accuracy pressure gauge (#63-5612).

10. Matheson Gas Products, 0-15 Psig, pressure gauge (#P/N 63-2215).

11. Harvard apparatus infussion pump.

12. a. Whitey, Micro-metering valve (#SS-21RS4)
    b. Matheson Gas Products, 0-60 Psig, 0.25% accuracy pressure gauge.

13. TSI Inc. model 3054 aerosol neutralizer.

14. Dwyer, Magnehelic 2-0-2 inches of water D/P gauge (#2304)

15. Whitey, 3-way ball valve (#SS-43XS4).

16. 3/8" nylon tubing.

17. Home made sampling probe, see Figure 14.

18. Climet Instruments, model CI-208 particle counter and model 316 printer.

19. Whitney, regulating valve (#SS-6LRS6).

20. The Lee Co., Lee Jet in fitting (#JETB1872200L).

21. Wallace and Tiernan, 0-800 mm Hg, aboslute pressure gauge (#61A-ID-0800).

22. Same as 8.

23. Same as 3.

APPENDIX B

Calibration curve for a sonic flow meter fixture, made of 2 orifices connected in parallel (total rating 100 Lohms).
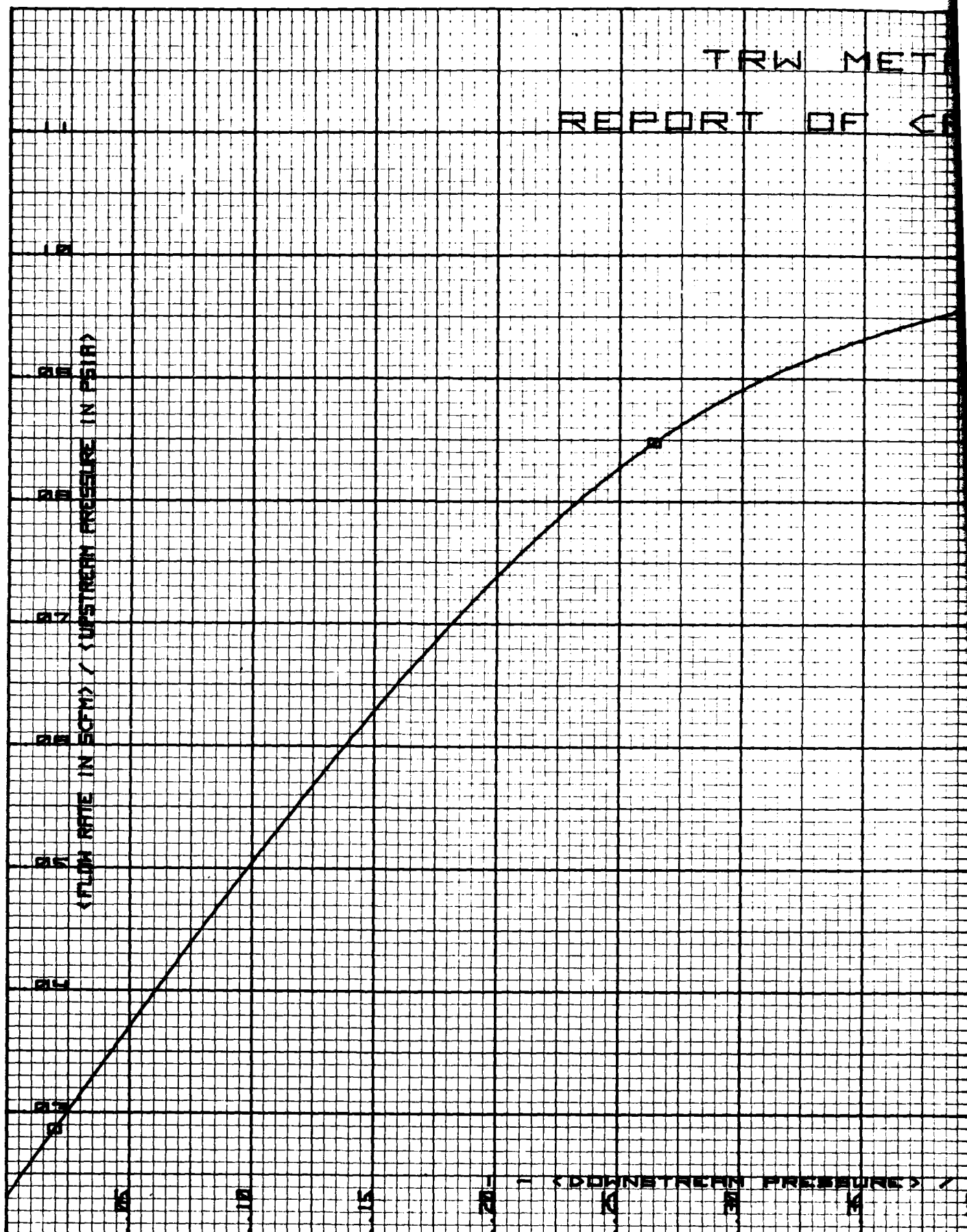
FIGURE B-1. SONIC ORIFICE C[

TROLOGY

CALIBRATION
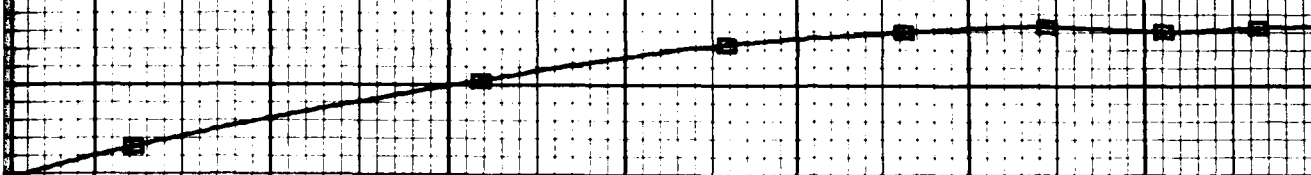
DESC = TWO PARALLEL JETS

MFR - THE LEE COMPANY

P/N - JEHB 1872 240L

TRW I.D. FIXTURE 1

TEST MEDIUM - AIR

TEST TEMP - 70 DEG F

STD TEMP - 70 DEG F

STD PRESSURE - 14.70 PSIA

DATE CALIB - 04/26/78

TESTED BY - L.L. BROWN 74

APPROVED - G.A. VELLUTINI

<UPSTREAM PRESSURE>

E CALIBRATION CURVE.   75

APPENDIX C

Vibrations of Circular Plates

The flexural rigidity of a circular plate clamped on the circumference is a cubic function of the thickness (Baumeister, 1976 p. 5-103),

$$D = Eh^3/12 (1 - \nu^2) . \tag{C-1}$$

The first fundamental frequency of vibration is

$$f = (\frac{\alpha}{2\pi a}) \sqrt{\frac{g}{d} \frac{D}{h}} . \tag{C-2}$$

Using (C-1) in equation (C-2),

$$f = (\frac{\alpha h}{2\pi a}) \sqrt{\frac{g}{12d(1 - \nu^2)} E} . \tag{C-3}$$

The vibration amplitude is inversely proportional to the frequency, and therefore to the plate thickness. It should be noted, though, that the plate diameter has a direct effect on the amplitude of vibration and optimization of the diameter and thickness may be useful.

In the above equation the following nomenclature is used:

a - radius of plate

b - specific weight of plate material

D - flexual rigidity

E - modulus of elasticity

g - gravitational acceleration

h - plate thickness

α - a constant

ν - Poisson's ratio

APPENDIX D

Calibration of Stage 0

An extra stage, similar in its geometry to stage one, was available for testing. It was attempted to operate this stage at a fractionation point around 7 μm. To do so, the jet nozzle diameter had to be increased to approximately 0.79 cm according to Equation (4). Since the inlet diameter to the tapered section of the nozzle is only 0.805 cm most of the inlet cone was eliminated by boring the nozzle. No other changes were made in the stage prior to testing, hence the S/D and the W/D ratios decreased by approximately 40%. The stage is named "Stage 0" since it has a fractionation point larger than that of stage one.

The above variations in geometry are found to be detremental to the operation of the CI, as shown on the data table below.

Table D-1: Crossover Efficiency and

Particle Loss in Stage 0 (DOP particles)

d_p, μm	2.3	2.9	3.32	3.65	4.45	8.5	9.0
η %	30.3	36.1	31.5	34.2	40.8	39.0	71.0
L %	0.0	0.0	0.0	0.0	9.0	44.7	74.0

While particle loss is virtually non-existant, the cross over efficiency of the state is poor for particles below the fractionation point. For particles larger than the fractionation point, very little data is

is available.   The reason being that most of the large aerosol generated

is lost before it can reach the CI.   This happens due to the vertical

upward position of the aerosol generator which makes it difficult to carry

heavy particles in a relatively low velocity stream coming out of the

generator.   To get around this problem the aerosol generator has to be

positioned upside down.

To improve the stage performance, it is believed that its geometry

has to be changed to correspond to the operating conditions of the other

two stages.   Explicitly, the spacing S/D, and the hole diameter in the

splitter plate W/D have to be corrected.   Also the tapered inlet

section of the nozzle has to be corrected and the nozzle length N/D

adjusted.

GLOSSARY

A_p - Frontal area of a particle.

C - Gas constant in Equation 45.

C - Cunningham slip correction factor.

C_1, C_2 - Constants of integration.

C_D - Drag Coefficient.

d_{aed} - Aerodynamic equivalent diameter.

d_p - Particle diameter.

D - Nozzle diameter.

D_1, D_2 - Diameter of the inlet and exit of the tapered nozzle section.

$D(x)$ - Diameter at distance x along the nozzle.

L - Stage particle loss.

L - Lohm, a unit of flow resistance, see Equation (45).

L_t - Total particle loss in a 2-stage CI.

ℓ - Spacing between the nozzle exit and the splitter plate.

m_p - Particle mass.

N - Length of the straight nozzle section.

P_1, P_2 - Pressure upstream and downstream of the sonic orifice.

Q - Volumetric flow rate.

Re - Reynolds number.

S - Length of the tapered nozzle section.

Stk - Stokes number, $\dfrac{\rho_p d_p^2 U}{9 \mu D}$

$Stk_{50\%}$ - Stokes number at the 50% cross-over efficiency.

T - Temperature.

t - time.

t^* - t/t_1.

t_1 - S/V_{g_1}.

U - Jet velocity.

V_{g_1}, V_{g_2} - Gas velocity at inlet and exit of the tapered nozzle section.

$V_g(x)$ - Gas velocity at distance x along the nozzle.

V_{p_1}, V_{p_2} - Particle velocity at inlet and exit of the tapered nozzle section.

V_g^* - V_g/V_{g_1}.

V_p^* - V_p/V_{g_1}

W - Diameter of hole in the splitter plate.

X - Coordinate along nozzle axis.

X_p - Particle location along nozzle axis.

$\dot{X}_p$ - Local particle velocity.

$\ddot{X}_p$ - Local particle acceleration.

α - $V_{g_2}^* - 1$.

γ_1, γ_2 - Constants defined by Equation 25.

ρ_g - Gas density.

ρ_p - Particle density.

ρ_p^* - Normalized density, ρ_p/ρ_1 where $\rho_1 = 1$ g/cc.

μ - Gas Viscosity.

η - Cross-over efficiency (1-stage CI).

η_c - Collection efficiency (2-stage CI).

$\cdot$ - Particle Characteristic time

$\cdot$ - $\cdot/t_1$

$\cdot$ Optical Particle Counter.

$\cdot$ Vibrating Orifice Monodispersed Aerosol Generator.

81

DISTRIBUTION LIST

Names	Copies
Chemical Systems Laboratory Aberdeen Proving Ground, MD 21010	
Office of the Director ATTN: DRDAR-CLG	1
Systems Development Division ATTN: DRDAR-CLY	4
CB Detection & Alarms Division ATTN: DRDAR-CLC	1
Developmental Support Division ATTN: DRDAR-CLJ-L ATTN: DRDAR-CLJ-R	3 2
Munitions Division ATTN· DRDAR-CLN ATTN: DRDAR-CLN-S	1 1
Physical Protection Division ATTN: DRDAR-CLW-P	1
Research Division ATTN: DRDAR-CLB ATTN: DRDAR-CLB-B ATTN: DRDAR-CLB-P ATTN: DRDAR-CLB-T ATTN: DRDAR-CLB-PS(Mr. Vervier) ATTN: DRDAR-CLB-PS(Dr. Stuebing) ATTN: DRDAR-CLB-PS(Mr. Doherty)	1 1 1 1 1 1 10

Department of Defense

Administrator Defense Documentation Center ATTN: Accessions Division Cameron Station Alexandria, VA 22314	2
Office of the Director Defense Research and Engineering ATTN: Dr. T. C. Walsh, Rm 3D-1079 Washington, DC 20310	1
Institute for Defense Analysis 400 Army-Navy Drive ATTN: L. Biberman ATTN: R. E. Roberts Arlington, VA 22202	1

DISTRIBUTION LIST CONT'D.

Names	Copies
Advanced Research Projects Agency 1400 Wilson Boulevard Arlington, VA 22209	1

Department of the Army

Commander
US Army Research Office - Durham   1
Box CM, Duke Station
Durham, NC 27706

HQDA (DAMO-SSC)   1
HQDA (DAMA-ARZ, Dr. Verderame)   1
HQDA (DAMA-CSM-CM)   1
HQDA (DAMI-FIT)   1
Washington, DC 20310

US Army Material Development and Readiness Command

Commander
US Army Material Development and Readiness Command
ATTN: DRCDE-DM   1
ATTN: DRCLDC   1
ATTN: DRCMT   1
ATTN: DRCSF-S   1
ATTN: DRCDL/Mr. N. Klein   1
ATTN: DRCBI/Col. Gearin   1
ATTN: DRCDMD-ST (Mr. T. Shirata)   1
5001 Eisenhower Ave.
Alexandria, VA 22333

Commander
US Army Foreign Science & Technology Center
ATTN: DRXST-ISI   1
ATTN: DRXST-CD/Mr. V. Rague   1
220 Seventh St., NE
Charlottesville, VA 22901

Commander
US Army Missile Command
Redstone Scientific Information Center
ATTN: Chief, Documents   1
ATTN: DRDMI-CGA (Dr. B. Fowler)   1
ATTN: DRDMI-TE (Mr. H. Anderson)   1
ATTN: DRDMI-KL (Dr. W. Wharton)   1
Redstone Arsenal, AL 35809

DISTRIBUTION LIST CONT'D.

Names	Copies

US Army Armament Research & Development Command

Commander
US Army ARRADCOM
ATTN: DRSAR-ASN — 1
ATTN: DRSAR-SA — 1
Dover, NJ 07801

Commander
Harry Diamond Laboratories
ATTN: DRXDO-RDC (Mr. D. Giglio) — 1
2800 Powder Mill Road
Adelphi, MD 20783

Chief, Office of Missile Electronic Warfare
US Army Electronic Warfare Laboratory
ATTN: DRSEL-WLM-SE (Mr. K. Larson) — 1
White Sands Missile Range, NM 88002

Project Manager for Smoke/Obscurants
ATTN: DRCPM-SMK — 2
ATTN: DRCPM-SMK — 1
ATTN: DRCPM-SMK-M/Tony Van de Wal — 1
ATTN: DRCPM-SMK-T — 1
Aberdeen Proving Ground, MD 21005

Commander
Atmospheric Sciences Laboratory
ATTN: DRSEL-BR-AS-P — 1
ATTN: DRSEL-BR-MS-A (Dr. R. Gomez) — 1
ATTN: DRSEL-BL-AS-DP (Mr. J. Lindberg) — 1
ATTN: DRSEL-BL-SY (Mr. F. Horning) — 1
ATTN: DRDEL-DR-AS-P — 1
ATTN: DELAS-BE-A — 1
White Sands Missile Range, NM 88002

Director
US Army Material Systems Analysis Activity
ATTN: DRXSY-D (Dr. Fallin) — 1
Aberdeen Proving Ground, MD 21005

Director
Night Vision Laboratories
ATTN: DRSEL-NV-VI (Mr. R. Moulton) — 1
ATTN: DRSEL-NV-VI (Mr. R. Bergemann) — 1
Fort Belvoir, VA 23651

Names	Copies

US Army Mobility Equipment Research & Development Center
ATTN: Code/DROME-RT (Mr. O. F. Kezer)   1
Fort Belvoir, VA 22060

Commander
US Army Electronics Command
ATTN: DRSEL-CT-1 (Dr. R. G. Buser)   1
ATTN: DRSEL-WL-S (Mr. J. Charlton)   1
Ft. Monmouth, NJ 07703

Director
US Army Material Systems Analysis Activity
ATTN: DRXSY-GS (Mr. Chernick)   1
ATTN: DRXSY-LA (Dr. Liu)   1
Aberdeen Proving Ground, MD 21005

Director
US Army Ballistic Research Laboratories
ATTN: DRXBR-DL (Mr. T. Finnerty)   1
ATTN: DRXBR-P (Mr. N. Gerri)   1
ATTN: DRDAR-BLB (Mr. R. Reitz)   1
ATTN: DRDAR-BLB (Mr. A. LaGrange)   1
Aberdeen Proving Ground, MD 21005

Cdr, APG
ATTN: STEAP-AD-R/RHA   1
ATTN: STEAP-TL   1
Aberdeen Proving Ground, MD 21005

Commander
US Army Test & Evaluation Command
ATTN: DRSTE-FA   1
Aberdeen Proving Ground, MD 21005

Commander
Dugway Proving Ground
ATTN: STEDP-PO   1
ATTN: Technical Library, Docu. Sec.   1
ATTN: STEDP-MT-DA-E   1
ATTN: STEDP-MT (Dr. L. Salamon)   1
Dugway, UT 84022

US Army Training & Doctrine Command

Commandant
US Army Infantry School
Combat Support & Maintenance Dept.
ATTN: NBC Division   1
Fort Benning, GA 31905

Names	Copies

Commandant
US Army Missile & Munitions Center & School
ATTN: ATSK-CD-MD   1
ATTN: ATSK-DT-MU-EOD   1
Redstone Arsenal, AL   35809

Commander
US Army Logistics Center
ATTN: ATCL-MM   1
Fort Lee, VA   23801

Commander
HQ, USA TRADOC
ATTN: ATCD-TEC (Dr. M. Pastel)   1
Fort Monroe, VA   23651

Commander
US Army Ordance and Chemical Center and School
ATTN: ATSL-CD-MS   1
ATTN: ATSL-CD-MS (Dr. T. Welsh)   1
Aberdeen Proving Ground, MD   21005

Department of the Navy

Commander
Naval Surface Weapons Center
ATTN: Tech Lib & Info Svcs Br   1
White Oak Laboratory
Silver Springs, MD   20910

Commander
Naval Intelligence Support Center   1
4301 Suitland Road
Washington, DC   20390

Commander
Naval Surface Weapons Center
Dahlgren Laboratory
ATTN: DX-21   1
Dahlgren, VA   22448

Commander
Naval Weapons Center
ATTN: Code 3311 (Dr. R. Bird)   1
ATTN: Code 382 (Dr. P. St. Amand)   1
ATTN: Code 3822 (Dr. Hindman)
China Lake, CA   93555

DISTRIBUTION LIST CONT'D.

Names	Copies
Commanding Officer Naval Weapons Support Center ATTN: Code 5041 (Mr. D. Johnson) Crane, IN 47522	1
Commander Naval Research Laboratory ATTN: Code 5709 (Mr. W. E. Howell) 4555 Overlook Avenue, SW Washington, DC 20375	1

Department of the Air Force

HQ, Foreign Technology Division (AFSC) ATTN: PDRR Wright-Patterson AFB, OH 45433	1
Commander Armament Development & Test Center ATTN: DLOSL (Technical Library) Eglin AFB, FL 32542	1
U.S. Army Material Systems Analysis Activity ATTN: DRXSY-MP Aberdeen Proving Ground, MD 21005	1
U.S. Army Armament Research and Development Command ATTN: DRDAR-TSS Dover, NJ 07801	5